
UNIVERSITÀ DEGLI STUDI DI ROMA

TOR VERGATA

Facoltà di Ingegneria

Corso di Laurea in Ingegneria Matematica


Tesi di Laurea Magistrale

# A Continuum Theory for the Natural Vibrations of Spherical Viral Capsids


Laureando
**Francesco Bonaldi**

Relatore
**Prof. Paolo Podio-Guidugli**

Correlatore
**Prof. Chandrajit Bajaj**
The University of Texas at Austin



A.A. 2011-2012

# Acknowledgements

I wish to thank my advisors, Professors Podio-Guidugli and Bajaj, who strongly believed in my potential and gave me the opportunity to spend three wonderful months in Austin, TX, working at this thesis. Thanks are due to Dr. Antonino Favata as well, who constantly followed my work.

# Contents

# Notation

We adopt the same notation as in [7]. We indicate both a function and its typical value by the same letter. In addition to the standard notation $\frac{\partial \Psi}{\partial z^i}$, at times we denote differentiation with respect to a coordinate by a comma followed by a subscript (usually, the index of the coordinate): for example, for $\Psi$ a scalar, vector or tensor field, its derivative with respect to coordinate $z^i$ will be denoted by $\Psi_{,i}$. The derivative of $\Psi$ with respect to time is denoted either by $\dot{\Psi}$ or by $\frac{\partial \Psi}{\partial t}$; the variation of $\Psi$ is denoted by $\delta\Psi$. We denote second-order tensors by bold-face capitals, vectors by bold-face, low-case letters, and scalars by light-face letters. We also make use of Einstein's summation convention, according to which the summation symbol is suppressed, and summation over all possible values of an index is signaled implicitly by the fact that it occurs twice in a monomial term. Greek indexes take the values 1 and 2, Roman indexes range from 1 to 3.

# Introduction

The goal of this work is to present a study of the natural vibrations of spherical viral capsids - we think, in particular, of the Satellite Tobacco Mosaic Virus (STMV) and of the Cowpea Chlorotic Mottle Virus (CCMV) - by employing a continuum mechanics approach.

We model such capsids as linearly elastic shells, whose response at any point is transversely isotropic with respect to the radial direction through that point (the simplest and most important subcase, isotropic response, is almost invariably considered in literature [9, 28]). Our choice is motivated by the desire to account for the rotational symmetries with respect to the radial direction of capsomers, the functional units a capsid consists of. In addition to transverse isotropy, the shell theory we employ has some other unusual traits. For one, due to the geometric and material heterogeneity of capsids, we allow both thickness and constitutive parameters to vary over a shell's middle surface. Moreover, while we presume the displacement field to be linear in the thickness coordinate, as is the case in the classical theories of Kirchhoff-Love and Reissner-Mindlin, at variance with those theories we allow for thickness distension.

There are two parts. Part I consists of Chapter 1, where we provide an overview about functions, geometry and mechanical modeling of viral capsids, and Chapters 2 to 4, where we offer a presentation of the mechanical theory of linearly elastic spherical shells we employ in this work to model spherical capsids, starting from the indispensable geometric preliminaries to cover kinematics, balance equations and constitutive issues, so as to arrive at general evolution

equations in terms of the displacement parameters and their derivatives. Part II consists of two more chapters. In Chapter 5, the evolution equations needed to analyze the natural vibrations of capsids are rewritten under the assumptions of homogeneous and isotropic response, and uniform thickness; moreover, the capsid is considered empty (that is, with no genome inside). Explicit analytical solutions are derived for axisymmetric vibrations, in the following special cases: radial vibrations without thickness changes, uniform radial vibrations with thickness changes, parallel-wise twist vibrations, and parallel-wise shear vibrations.

Yang et al. [28] schematized the STMV capsid as a three-dimensional continuous elastic isotropic body; in order to infer the value of the Young's modulus $E$ of the capsid, they took for the Poisson's ratio a value close to that of bulk soft matter ($\nu = 0.3$), and equated the expression for the longitudinal sound speed in a three-dimensional isotropic body of generic shape to the numerical value of this speed measured in STMV crystals by Brillouin scattering experiments [24]. We believe this to be a questionable procedure, because the shell-like geometry of the capsid is not taken into account. Instead, the explicit formulae we derived for the types of vibrational frequencies listed just above might be used to obtain a correct estimate of Young's modulus and Poisson's ratio of the STMV capsid, as well as of any spherical capsid susceptible of being modeled as homogeneous and isotropic, in case experiments were run, where the corresponding vibrational modes are induced.

Our last Chapter 6 is devoted to delineate some directions for future research along the lines we have chosen, in particular, to a study of the complex pressure loading a capsid shell is subject to when genome-filled and immersed in a hydrostatic environment, a loading that is classified as 'live', in that at the same time it depends on and determines the motion of the shell.

# Chapter 1

# Viral Capsids

## 1.1 Functions, Structure, Nomenclature

Viral capsids are self-assembled nanometre-size protein shells whose main functions are to enclose and protect the genetic materials (DNA or RNA) of viruses in one host cell, to transport and to release those materials inside another host cell. Being tightly packed into the capsid, the genome exerts a pressure on it, that the capsid is designed to withstand.

A capsid consists of several structural subunits, the *capsomers*, made up by one or more individual proteins and held together by non-covalent forces so as to form very regular structures that are, in most cases, either helical or icosahedral[1]. According to its capsomer structure, the shape of a capsid approximates, respectively, that of a cylinder and of a sphere. For this reason, helical and icosahedral capsids are often referred to as, respectively, *cylindrical* and *spherical* capsids and, at the macroscopic scale, can be regarded as cylindrical and spherical shells. Typical examples of viruses with spherical capsids, both largely studied in the literature, are the Satellite Tobacco Mosaic Virus (STMV, Fig. 1.1) [8, 13, 14, 24] and the Cowpea Chlorotic Mottle Virus (CCMV, Fig. 1.2) [3, 9, 16, 25, 26]; on the other hand, a classical example of

[1]The terms "capsid" and "capsomers" were proposed by Lwoff, Anderson and Jacob in 1959 [15].

cylindrical viral capsid is the Tobacco Mosaic Virus capsid (TMV, Fig. 1.3). In the sequel, we shall deal only with spherical (icosahedral) capsids.

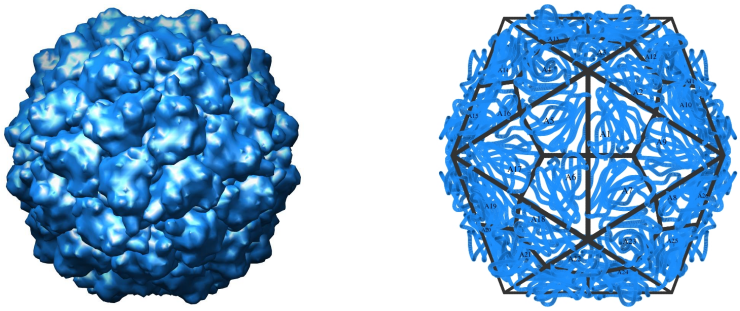

Figure 1.1: STMV capsid and arrangement of its subunits.

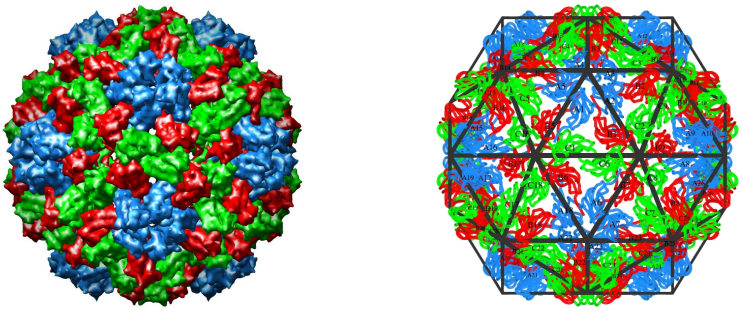

Figure 1.2: CCMV capsid and arrangement of its subunits.

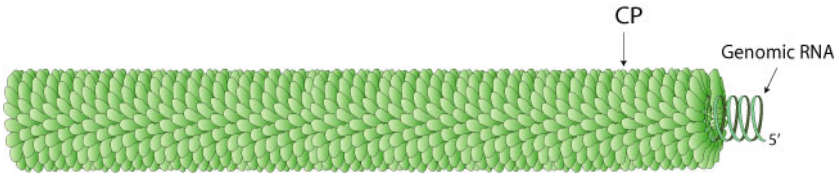


Figure 1.3: TMV: capsid and genome.

Recall that an *icosahedron* (Fig. 1.4) – one of the five Platonic solids – is a regular polyhedron with 20 identical equilateral triangular faces, 30 edges and 12 vertices, showing three-, two- and five-fold symmetry, respectively. A two-fold symmetry axis passes through the midpoint of each edge, a three-fold axis through the center of each face, and a five-fold axis through each vertex [2].

The simplest icosahedral capsid is built up by using 3 identical protein

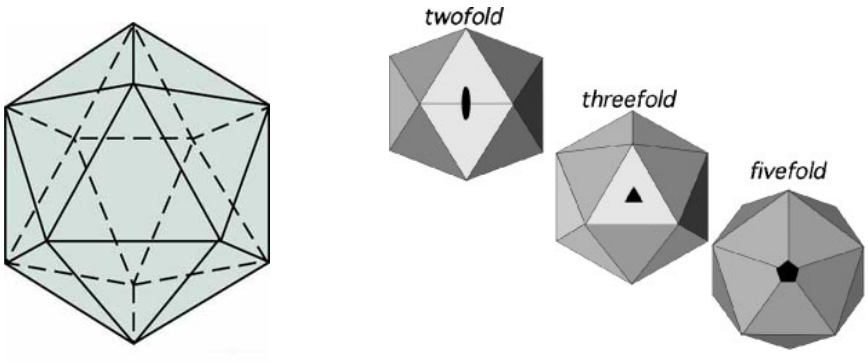


Figure 1.4: The icosahedron and its symmetries.

subunits to form each triangular face, thereby requiring 60 identical subunits in total. However, not all capsids contain only 60 subunits. Some form larger structures, while still keeping the overall icosahedral symmetry. There are many ways to distribute proteins on a surface in accordance with icosahedral symmetry and these can be described in terms of tessellations. The first example of tessellation applied to viral capsids was given by Caspar and Klug [5] in 1962. Their main idea was that the protein subunits occupy *quasi-equivalent* positions on the viral capsid: this means that the individual subunits, in larger capsids, retain the basic bonding properties, but occupy slightly different environments. This is realized by the sub-triangulation of each face of the icosahedron into smaller triangular facets, as we shall point out shortly.

The capsomers in a spherical capsid are classified as *pentamers* and *hexamers*, according to whether their rotational symmetries are, respectively, five-fold or six-fold. Whatever the size of the capsid, since pentamers always occupy the vertices of the icosahedron, their number is constant and equal to 12; on the other hand, the number of hexamers, along with the selection rules of their distribution on a surface lattice, depends on the size of the icosahedron, which is determined by the so called *triangulation number* ($T$-number) [2, 5, 30], a notion that we now introduce.

Consider a hexagonal plane lattice (Fig. 1.5), and choose the center of a

hexagon as the origin; with reference to the $h$ and $k$ axes, the centers (lattice points) of all other hexagons have coordinates $(h, k)$, with both $h$ and $k$ relative integers. Let $L$ be the distance between the origin and a generic lattice point.

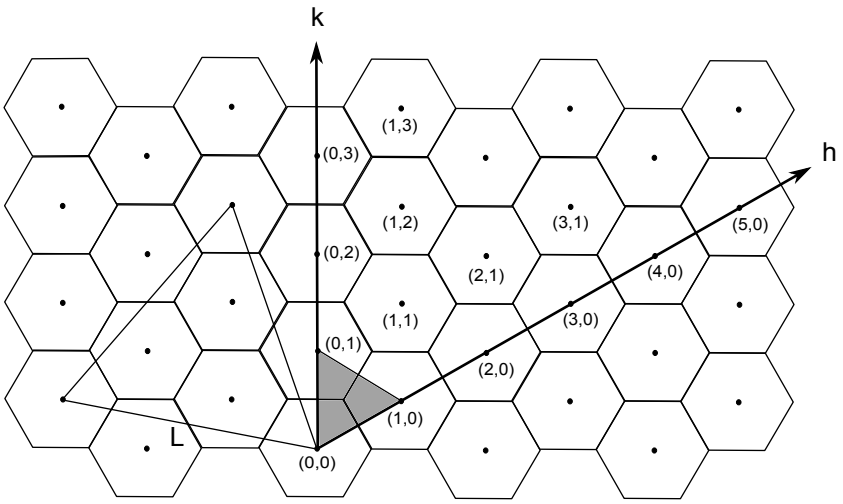


Figure 1.5: Hexagonal plane lattice.

In three dimensions, a lattice point corresponds to a vertex of the icosahedron, $L$ to the length of its edge, and the equilateral triangle of side $L$ to a single face. Thus, the size of the icosahedron depends on which lattice point one chooses to be the vertex closest to the origin. If $(h, k) = (1, 0)$ (shaded triangle), an icosahedron consisting solely of pentamers is formed; in all other cases, such as $(h, k) = (1, 1)$, hexamers shall be present as well (figs. 1.6, 1.7). In terms of the lattice coordinates, it results

$$L^2 = h^2 + hk + k^2.$$

The area of the equilateral triangle of side $L$ divided by the area of an equilateral triangle of unit side (like the shaded triangle in Fig. 1.5) yields the triangulation number:

$$T = \frac{\frac{\sqrt{3}}{4}L^2}{\frac{\sqrt{3}}{4}} = h^2 + hk + k^2.$$

Thus, the $T$-number is the number of unit-side equilateral triangles (facets)

each face of the icosahedron can be split into. It can assume only certain integer values (1, 3, 4, 7, 9, 12, 13, ...).

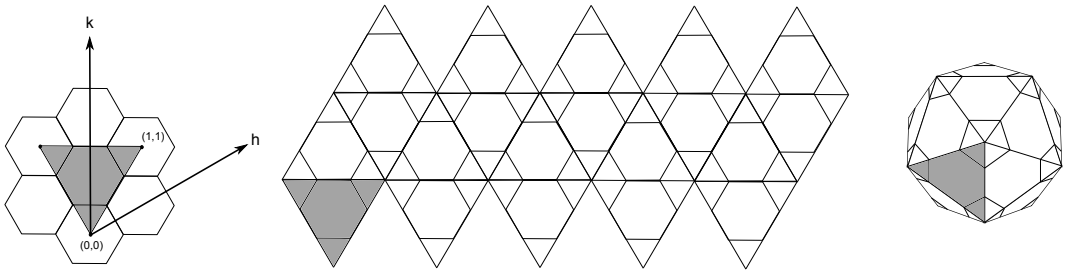


Figure 1.6: Construction of an icosahedron with $T = 3$: $(h, k) = (1, 1)$.

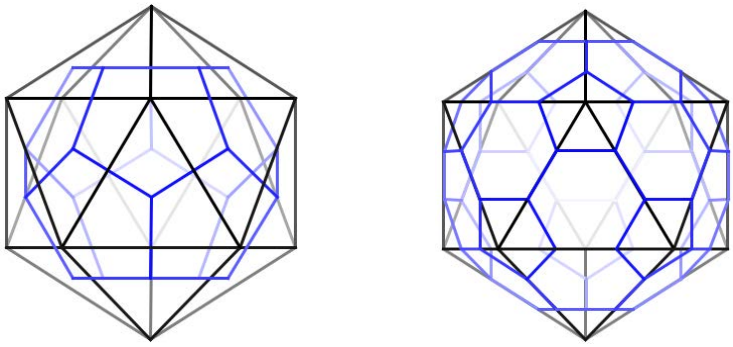

Figure 1.7: $T = 1$ capsid (left) and $T = 3$ capsid (right) surfaces, viewed from a three-fold axis: the presence of hexamers, in addition to pentamers, is clearly remarked in the second case.

Since three proteins can be arranged in each of the $20T$ facets, the total number of proteins in an icosahedral capsid is equal to $60T$, whereof 60 are clustered into the 12 pentamers and $60(T - 1)$ are clustered into hexamers; hence, the total number of hexamers is equal to $10(T - 1)$. As to the two examples mentioned above, the capsid of the STMV, one of the smallest viruses known, is characterized by a triangulation number $T = 1$ and thus is made up of 60 copies of a single protein, clustered into the 12 pentamers, without any hexamer; the CCMV capsid has, on the other hand, triangulation number $T = 3$ and is made up of 180 copies of a single protein, clustered into 12 pentamers and 20 hexamers.

## 1.2 Geometry, Material Moduli

The capsomers form protrusions from the capsid surface, making the shell's thickness non-uniform [9]. Supposing that an ideal value $t_{\mathcal{I}}$ of the thickness of an icosahedral capsid could be determined (for example, by calculating its average from the information available in the Protein Data Bank), the thickness $t_{\mathcal{S}}$ of the spherical shell representing the capsid can be calculated by assuming equality of the volumes of the two shell-like regions. Denote the area of the capsid surface (icosahedron) by $A_{\mathcal{I}}$, and consider the sphere circumscribed to the icosahedron as the middle surface of the spherical shell, whose area we denote by $A_{\mathcal{S}}$; then,

$$t_{\mathcal{S}} = \frac{A_{\mathcal{I}}\, t_{\mathcal{I}}}{A_{\mathcal{S}}}. \tag{1.1}$$

Recall that, given the radius $\rho_o$ of the circumscribed sphere, the length $L$ of the edge of the icosahedron is

$$L = \frac{\rho_o}{5}\sqrt{10\left(5-\sqrt{5}\right)}\,; \tag{1.2}$$

the area of the icosahedron, on the other hand, is

$$A_{\mathcal{I}} = 5\sqrt{3}\,L^2\,; \tag{1.3}$$

substitution of (1.2) into (1.3) yields

$$A_{\mathcal{I}} = 2\sqrt{3}\left(5-\sqrt{5}\right)\rho_o^2\,,$$

therefore, since $A_{\mathcal{S}} = 4\pi\rho_o^2$, (1.1) becomes

$$t_{\mathcal{S}} = \frac{\sqrt{3}\,(5-\sqrt{5})}{2\pi}\,t_{\mathcal{I}} \approx 0.76\,t_{\mathcal{I}}.$$

Yang et al. [28] inferred the values of the ideal inner and outer radii of the

spherical shell representing the STMV capsid – which we will take as a reference in the sequel – from the graphical representation of the variation of the mass distribution with respect to the radial coordinate; namely, they considered the values of the radial coordinate corresponding to the first and last peaks of that variation, i.e., $R_1 = 55.4\,\text{Å}$ and $R_2 = 86\,\text{Å}$ (Fig. 1.8), whence the values $t_{\mathcal{S}} = 30.6\,\text{Å}$ for the ideal uniform thickness and $\rho_o = 70.7\,\text{Å}$ for the radius of the middle surface of the spherical shell.

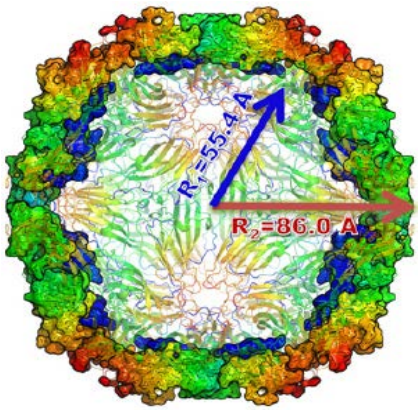


Figure 1.8: Cross-sectional view of the STMV capsid.

The mass density of the shell is obtained by simply dividing the total mass, calculated from the data available in the Protein Data Bank, by the volume, and turns out to have the value $\delta_o = 823.82\ \text{kg/m}^3$. As to the elastic moduli, Brillouin scattering measurements [24] were performed on hydrated and dehydrated crystals of STMV, yielding values of the longitudinal sound speed that range from 1920 m/s to 3350 m/s, respectively. The longitudinal sound speed $c_l$ in a three-dimensional isotropic elastic continuous body has the following expression in terms of the Young's modulus $E$ and the Poisson's ratio $\nu$:

$$c_l = \sqrt{\frac{E(1-\nu)}{\delta_o(1+\nu)(1-2\nu)}}\,; \tag{1.4}$$

assuming that the anisotropy of the crystalline structure is weak and that the Poisson's ratio of viruses is close to that of soft condensed matter, i.e., $\nu = 0.3$,

then, by (1.4), the values of the Young's moduli corresponding to the above sound speeds are, respectively, $E_1 = 3.7\,\mathrm{GPa}$ (for fully hydrated samples) and $E_2 = 11.2\,\mathrm{GPa}$ (for fully dehydrated samples). However, these values are obtained using the expression of the longitudinal sound speed in a continuous body of general shape, not of shell-like shape, like the STMV capsid; in fact, (1.4) involves only the density of the shell, but none of its geometrical features, such as the thickness and the radius of the middle surface.

As to the CCMV capsid, Speir et al. [23] performed measurements of the maximum and minimum values of the outer and inner radii, using X-ray crystallography and cryo-electron microscopy techniques; Gibbons and Klug [9] considered the average values of the results of those measurements, namely, $R_1 = 10.4\,\mathrm{nm}$ and $R_2 = 13.2\,\mathrm{nm}$, as the values of the ideal inner and outer radii of the spherical shell they suppose to represent the capsid, whence the ideal thickness $t_{\mathcal{S}} = 2.8\,\mathrm{nm}$ and the radius of the middle surface $\rho_o = 11.8\,\mathrm{nm}$. To infer the mechanical properties of the CCMV capsid, atomic force microscopy nanoindentation studies were performed [16], yielding values of the Young's modulus equal to $E_1 = 140\,\mathrm{MPa}$ for the wild-type capsid and $E_2 = 190\,\mathrm{MPa}$ for the mutant one; as to the Poisson's ratio $\nu$, since proteins tend to behave as if they were almost incompressible [9], it is reasonable to assume a value $\nu = 0.4$. The value of the Poisson's ratio was actually shown not to be so influential on the mechanical response of the capsid.

## 1.3 Mechanical Modeling

Bottom-up models of viral capsids have been built in the frameworks of both molecular dynamics (MD) and normal mode analysis (NMA) [1, 6, 25], and used to study free vibrations [10]. Recently, certain top-down models based on two- and three-dimensional continuum elasticity have provided a theoretical complement to single molecule experiments such as atomic force microscopy

(AFM), and have advanced the fundamental understanding of the mechanics of these structures when they are subject to external forces.

In particular, Gibbons and Klug [9] have modeled the CCMV capsid as a three-dimensional homogeneous and isotropic elastic body, and explored what predictions would follow from adopting one or another of three different non-linear constitutive laws (namely, St. Venant-Kirchhoff's, Mooney-Rivlin's and Neo-Hookean) when simulating AFM nanoindentation experiments. They found that the capsid's force response to indentation is quite insensitive to constitutive details, and greatly influenced by geometry. To justify their employment of a three-dimensional elasticity model, they asserted that "the nominal thickness of CCMV is just over 10% of its outer diameter, likely putting it outside the range of applicability for thin-shell analysis. Two options remain for analysis of a thick shell like the CCMV capsid. The first is to resort to shell theories which allow for shear deformation, and the second is to work within the general framework of 3D continuum elasticity. In the present work, focus is on the latter, more general approach".

In another paper [11], Gibbons and Klug point out the influence of the capsid's non-uniform geometry on its mechanical response. They provide a detailed elucidation of the CCMV capsid's structure and write down explicitly the expressions of the constructs used in the mechanical modeling, namely, the non-linear and exact strain measure, the stored elastic energy and the stress measure, given by the derivative of the elastic energy with respect to the strain measure; the constitutive law employed is Neo-Hookean (linear in the first invariant of the strain measure), extended to the compressible range by addition to the standard expression for the elastic energy of a term that features the logarithm of the determinant of the strain measure. In the same paper, attention is drawn to the fact that the CCMV's mechanical response should be modeled as depending on pH, given that the CCMV can undergo a pH-controlled conformational change in the form of a diffused swelling. Models of both native

and swollen CCMV capsids are generated from X-ray crystal structures, and used in finite element simulations of AFM indentation along two-, three-, and five-fold icosahedral symmetry orientations. The force response of the swollen capsid model is found to be softer by roughly a factor of two, significantly more non-linear and more orientation-dependent than that of a native capsid with equivalent elastic moduli. These findings are taken as a demonstration that a capsid's geometric heterogeneity can have significant effects on its global structural response.

Bajaj et al. [3] provided two heterogeneous models of the CCMV capsid, again in the framework of three-dimensional continuum mechanics. These models were called the *heterogeneous continuous model* and the *heterogeneous spring model*; they are refined versions of the homogeneous continuous model set forth in [9] and [11], and aim to account for the difference in interaction due to bonded and non-bonded forces (the former acting within the capsomers, the latter acting between them) and to better capture the non-uniform geometry and material properties of the capsid. The inter-capsomers region is modeled as a "pseudo-material", characterized by a certain Young's modulus and a certain Poisson's ratio, in the heterogeneous continuous model; and as a collection of elastic springs with a certain overall elastic constant in the spring-based model. A comparison between the results yielded by these two models and the homogeneous continuous model is presented, showing how the two refined models better reflect the non-linear force-indentation behavior of the capsid observed experimentally; furthermore, the stiffness of the inter-capsomers region is observed to be much higher than that of the capsomers material itself, and the Young's modulus of that region is higher than the overall elastic constant of the spring model; this is expected since the heterogeneous continuous model represents a generalization of the spring-based model, and the Young's modulus of the gap region can be viewed as an infinite sum of infinitesimal elastic spring constants. Consequently, in the nanoindentation process, the deforma-

tion is mainly undergone by the capsomers, whereas their change in relative position is not so important: only relative rotations between capsomers contribute to the deformation of the capsid. The stiffness of the pseudo-material between the capsomers in the heterogeneous continuous model and the overall elastic constant in the spring-based model are estimated by tuning simulation parameters, until the output matches the experimental results. The authors' study also shows that the non-linear force response of the capsids to indentation is insensitive to the internal molecular dynamics of the proteins, implying that the continuum approach is valid; however, it is influenced by the capsid's geometry.

Ru [22] built a mechanical model of a spherical capsid by using the *Reissner-Mindlin*'s shell theory [17] (Section 3.1.1): transverse shear deformations are allowed because the terms multiplied by the thickness coordinate in the expressions of the in-plane scalar displacements are arbitrary functions of the spherical coordinates; also, since the radial displacement does not depend on the thickness coordinate, thickness distension is forbidden. A key feature of Ru's model is that the transverse shear modulus of capsids is allowed to be much lower than their in-plane shear modulus, in accordance with the weak resistance of two-dimensional protein assemblies to transverse shear. The in-plane stress-strain relations are derived by integration over the thickness of the three-dimensional isotropic constitutive laws. Another feature of Ru's model is the employment of an *effective bending thickness* $h_0$, in place of the average thickness $h$, in the expressions of the bending rigidities. This is because, as Ru states, "[...] further work needs to be done on calculating and measuring the bending modulus of viral capsids which plays a central role in viral shell mechanics. For microtubules, for instance, it has been showed that bending rigidities are determined by an effective bending thickness $h_0 = 1.6$ nm, which is much smaller than the average thickness $h = 2.7$ nm. Therefore, the present model allows the effective bending thickness $h_0$ to be different from the average thickness $h$ [...]". The results pro-

vided in the paper suggest that the classical homogeneous shell model widely used in the literature would overestimate the strength of viral shells against buckling under external pressure. Ru's model could extend the applicability of homogeneous elastic shell models from large-radius viral shells to small-radius ones as well, since the effect of transverse shear is more significant for the latter than for the former.

Analysis of the mechanical properties of viral capsids has also been made by Tama and Brooks [25] performing normal mode analysis, based on the Elastic Network Model [1]. Application of the standard atomic-level procedure for NMA entails calculation and diagonalization of the Hessian matrix of the potential energy, whose size is $3N$, with $N$ the number of atoms in the system. Such diagonalizations are impossible for virus particles represented with complete atomic detail, and even with coarse-grained models taking into account only the $C^{\alpha}$ atoms, due to their enormous size; thus, methods to reduce the effective size of the system are needed. For a further reduction of the Hessian matrix, the authors used the rotation-translation-blocks method, which gives a good approximation for the low-frequency normal modes. These methods are successful because the global mechanical properties of the molecule being studied are sensitive mainly to the mass distribution of the molecule, i.e., the lowest frequency modes of a molecule can be well represented by analyzing a continuum elastic body with analogous mass distribution. This is exactly what Yang et al. did [28]. In this paper, the authors "carry coarse-graining to its extreme" and employ a continuum-mechanical model to perform vibrational analysis of a variety of systems with spherical symmetry, including the STMV capsid (both empty and filled with the viral genome), assuming the material to be elastic, linear, homogeneous and isotropic. Quantization of the vibrational frequencies follows from the boundary condition that the surface contact forces applied on the inner and outer surfaces of the capsid be equal to zero.

In the present work, we perform an analysis of natural vibrations of a spher-

ical capsid, within the framework of linear mechanics of elastic structures. As in Ru's model, we schematize a capsid as a linearly elastic spherical shell; but, unlike for all modeling efforts summarized in the above paragraphs, we allow for a mechanical response that (*i*) is inhomogeneous, in that, although fiber-wise constant, it may vary over middle surface of the shell; and that (*ii*) is transversely isotropic with respect to the radial direction through each point of that surface. The motivation of choosing such a response is related, respectively, to the material and geometric heterogeneity of capsids and to the properties of rotational symmetry of the pentamers and the hexamers with respect to the radial direction (five-fold and six-fold); in fact, we expect such symmetry properties to affect the mechanical behavior as well. Two other distinctive elements of our approach are that (*iii*) we let the shell thickness vary over the middle surface; and that (*iv*) we allow for both transverse shear deformation and thickness distension. Consequently, our theory is more general than the Reissner-Mindlin's shell theory employed by Ru.

# Part I

# Linearly Elastic Spherical Shells

# Chapter 2

# Geometry

We omit details about the general theory regarding the geometry of shell-like regions; those details are set forth in [7], to which we refer for further deepening. Here we recollect the main features about the geometry of spherical shells.

## 2.1 Local Bases

Let $\mathcal{E}$ be a three-dimensional Euclidean space, $\mathcal{V}$ its associated vector space, and let $x$ denote the typical point of the middle surface $\mathcal{S}$ of a spherical shell. We choose an origin $o \in \mathcal{E}$ and denote by $\boldsymbol{x} := x - o$ the position vector of $x$ with respect to $o$. Let $\{o; \boldsymbol{c}_1, \boldsymbol{c}_2, \boldsymbol{c}_3\}$ be a cartesian frame for $\mathcal{E}$ and $z^1 = \vartheta$, $z^2 = \psi$ be the curvilinear coordinates over $\mathcal{S}$ (Fig. 2.1). Defining $\mathrm{S} := (0, \pi) \times (0, 2\pi)$, the middle surface admits the global one-to-one parametrization given by

$$\begin{aligned} \mathrm{S} \ni (\vartheta, \psi) \mapsto x = x(\vartheta, \psi) = o + \boldsymbol{x}(\vartheta, \psi) \in \mathcal{S}, \\ \boldsymbol{x}(\vartheta, \psi) = \rho_o(\sin\vartheta\, \boldsymbol{c}(\psi) + \cos\vartheta\, \boldsymbol{c}_3), \\ \boldsymbol{c}(\psi) = \cos\psi\, \boldsymbol{c}_1 + \sin\psi\, \boldsymbol{c}_2. \end{aligned} \tag{2.1}$$

We write the inverse of mapping (2.1) as

$$\mathcal{S} \ni x \mapsto (\vartheta, \psi) = (\vartheta(x), \psi(x)) \in \mathrm{S}.$$

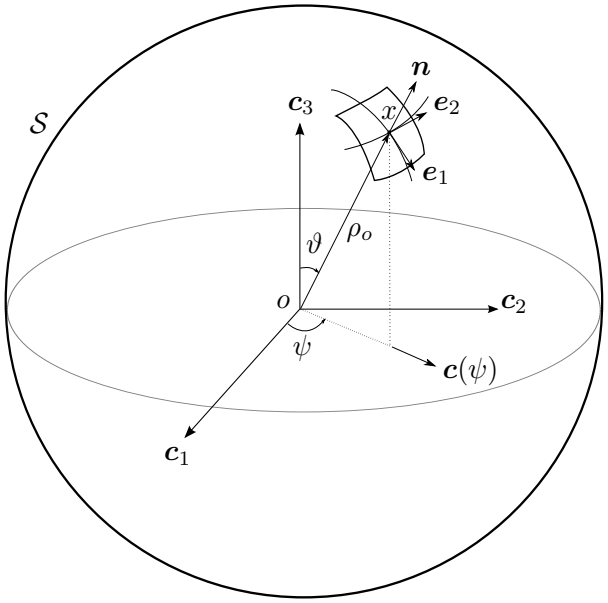


Figure 2.1: Geometrical equipment of the middle surface of a spherical shell.

Given $\varepsilon > 0$, the *shell-like region* $\mathcal{G}(\mathcal{S}, \varepsilon)$ of thickness $2\varepsilon$, modeled over $\mathcal{S}$ (Fig. 2.2), admits a global parametrization involving a system of *normal coordinates*: $z^1 = \vartheta$, $z^2 = \psi, z^3 = \zeta$, the last one being the coordinate along the direction given by $\boldsymbol{n}$, the outer unit normal vector field over $\mathcal{S}$:

$$\begin{gathered} \mathrm{S} \times I \ni (\vartheta, \psi, \zeta) \mapsto p = p(\vartheta, \psi, \zeta) = o + \boldsymbol{p}(\vartheta, \psi, \zeta) \in \mathcal{G}(\mathcal{S}, \varepsilon), \\ \boldsymbol{p}(\vartheta, \psi, \zeta) = \boldsymbol{x}(\vartheta, \psi) + \zeta \boldsymbol{n}(\vartheta, \psi). \end{gathered} \tag{2.2}$$

Setting $I := (-\varepsilon, +\varepsilon)$, we identify $\mathcal{G}(\mathcal{S}, \varepsilon)$ with the cartesian product $\mathcal{S} \times I$, and thus write $p \equiv (x, \zeta)$.

**Remark 1.** The thickness may vary with point $x \in \mathcal{S}$. We will left tacit this dependence in the following developments, and write $\varepsilon = \varepsilon(x)$.

We call

$$\mathcal{S}_h := \{p \in \mathcal{G}(\mathcal{S}, \varepsilon) : p = o + \boldsymbol{p}(\vartheta, \psi, h)\},$$

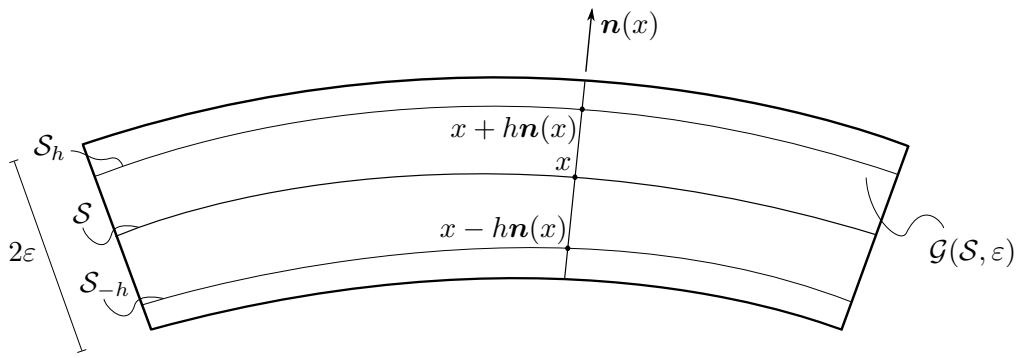


Figure 2.2: Section of a shell-like region with uniform thickness, modeled over the middle surface $\mathcal{S}$ ($0 < h < \varepsilon$).

the surface parallel to $\mathcal{S}$ corresponding to $\zeta = h$; also, for fixed $x \in \mathcal{S}$, we define

$$\mathcal{F}(x) := \{p \in \mathcal{G}(\mathcal{S}, \varepsilon) : p = x + \zeta \boldsymbol{n}(x),\, \zeta \in I\}\,,$$

the *material fiber* passing through $x$. The *tangent plane* to $\mathcal{S}$ at point $x$ is defined by

$$\mathcal{T}_x(\mathcal{S}) := \{q \in \mathcal{E} : (q - x) \cdot \boldsymbol{n}(x) = 0\}\,;$$

the tangent plane to $\mathcal{S}_h$ at point $p_h := x + h\boldsymbol{n}(x)$, parallel to $\mathcal{T}_x(\mathcal{S})$, is denoted by $\mathcal{T}_{p_h}(\mathcal{S}_h)$ and defined analogously.

For any point $x \in \mathcal{S}$, i.e., for any pair $(\vartheta, \psi) \in \mathrm{S}$, we can define three different bases for the vector space $\mathcal{V}$ associated with $\mathcal{E}$. The *covariant basis* is given by $\{\boldsymbol{e}_1(\vartheta,\psi), \boldsymbol{e}_2(\vartheta,\psi), \boldsymbol{e}_3(\vartheta,\psi)\}$, where[1]

$$\begin{aligned}
\boldsymbol{e}_1(\vartheta,\psi) &:= \frac{\partial \boldsymbol{x}}{\partial \vartheta}(\vartheta,\psi) = \rho_o(\cos\vartheta\, \boldsymbol{c}(\psi) - \sin\vartheta\, \boldsymbol{c}_3),\\
\boldsymbol{e}_2(\vartheta,\psi) &:= \frac{\partial \boldsymbol{x}}{\partial \psi}(\vartheta,\psi) = \rho_o \sin\vartheta\, \boldsymbol{c}'(\psi),\\
\boldsymbol{e}_3(\vartheta,\psi) &:= \frac{\boldsymbol{e}_1(\vartheta,\psi) \times \boldsymbol{e}_2(\vartheta,\psi)}{|\boldsymbol{e}_1(\vartheta,\psi) \times \boldsymbol{e}_2(\vartheta,\psi)|} = \boldsymbol{n}(\vartheta,\psi) = \rho_o^{-1}\boldsymbol{x}(\vartheta,\psi) = \sin\vartheta\, \boldsymbol{c}(\psi) + \cos\vartheta\, \boldsymbol{c}_3;
\end{aligned}$$

[1] Here, a prime denotes differentiation with respect to $\psi$.

the *contravariant basis* is given by $\{\boldsymbol{e}^1(x), \boldsymbol{e}^2(x), \boldsymbol{e}^3(x)\}$, where[2]

$$\begin{aligned}
\boldsymbol{e}^1(x) &:= {}^{\mathrm{s}}\nabla\vartheta(x) = \frac{1}{\rho_o^2}\boldsymbol{e}_1(\vartheta(x), \psi(x)),\\
\boldsymbol{e}^2(x) &:= {}^{\mathrm{s}}\nabla\psi(x) = \frac{1}{\rho_o^2 \sin^2\vartheta(x)}\boldsymbol{e}_2(\vartheta(x), \psi(x)),\\
\boldsymbol{e}^3(x) &:= \boldsymbol{n}(x).
\end{aligned}$$

A vector field $\boldsymbol{v}$ defined over $\mathcal{S}$ can be represented both in the covariant basis and in the contravariant basis:

$$\boldsymbol{v} = v_i\boldsymbol{e}^i = v^j\boldsymbol{e}_j, \quad \text{with} \quad v_i := \boldsymbol{v}\cdot\boldsymbol{e}_i, \quad v^j := \boldsymbol{v}\cdot\boldsymbol{e}^j \quad (i,j=1,2,3).$$

Analogously, a second-order tensor field $\boldsymbol{T}$ can be represented as

$$\boldsymbol{T} = T^{ij}\boldsymbol{e}_i\otimes\boldsymbol{e}_j = T_{ij}\boldsymbol{e}^i\otimes\boldsymbol{e}^j = T^i_j\boldsymbol{e}_i\otimes\boldsymbol{e}^j = T^j_i\boldsymbol{e}^i\otimes\boldsymbol{e}_j,$$

in terms of its covariant, contravariant, or mixed components: $T_{ij} := \boldsymbol{T}\cdot\boldsymbol{e}_i\otimes\boldsymbol{e}_j$, $T^{ij} := \boldsymbol{T}\cdot\boldsymbol{e}^i\otimes\boldsymbol{e}^j$, $T^i_j := \boldsymbol{T}\cdot\boldsymbol{e}^i\otimes\boldsymbol{e}_j$ and $T^j_i := \boldsymbol{T}\cdot\boldsymbol{e}_i\otimes\boldsymbol{e}^j$.

Since we use an orthogonal coordinate system, i.e., $\boldsymbol{e}_1\cdot\boldsymbol{e}_2 = 0$, we can define the *physical basis* $\{\boldsymbol{e}_{<1>}(\vartheta,\psi), \boldsymbol{e}_{<2>}(\vartheta,\psi), \boldsymbol{e}_{<3>}(\vartheta,\psi)\}$, a basis made of mutually orthogonal unit normal vectors, as follows:

$$\begin{aligned}
\boldsymbol{e}_{<1>}(\vartheta,\psi) &:= \frac{\boldsymbol{e}_1(\vartheta,\psi)}{|\boldsymbol{e}_1(\vartheta,\psi)|} = \frac{\boldsymbol{e}^1(x(\vartheta,\psi))}{|\boldsymbol{e}^1(x(\vartheta,\psi))|} = \cos\vartheta\,\boldsymbol{c}(\psi) - \sin\vartheta\,\boldsymbol{c}_3,\\
\boldsymbol{e}_{<2>}(\vartheta,\psi) &:= \frac{\boldsymbol{e}_2(\vartheta,\psi)}{|\boldsymbol{e}_2(\vartheta,\psi)|} = \frac{\boldsymbol{e}^2(x(\vartheta,\psi))}{|\boldsymbol{e}^2(x(\vartheta,\psi))|} = \boldsymbol{c}'(\psi),\\
\boldsymbol{e}_{<3>}(\vartheta,\psi) &:= \boldsymbol{n}(\vartheta,\psi) = \sin\vartheta\,\boldsymbol{c}(\psi) + \cos\vartheta\,\boldsymbol{c}_3.
\end{aligned}$$

The advantage of having defined a physical basis is that all of the components of any tensor or vector field along the elements of such a basis have the same physical dimensions, unlike the covariant and contravariant components of that field. Thus, for $\boldsymbol{v}$ and $\boldsymbol{T}$ respectively a vector and tensor field over $\mathcal{S}$, we can

[2] Here ${}^{\mathrm{s}}\nabla$ denotes the surface gradient.

write

$$\boldsymbol{v} = v_{<i>}\,\boldsymbol{e}_{<i>}, \quad \boldsymbol{T} = T_{<ij>}\,\boldsymbol{e}_{<i>} \otimes \boldsymbol{e}_{<j>} \quad (i,j=1,2,3),$$

where $v_{<i>} := \boldsymbol{v}\cdot\boldsymbol{e}_{<i>}$ and $T_{<ij>} := \boldsymbol{T}\cdot\boldsymbol{e}_{<i>}\otimes\boldsymbol{e}_{<j>}$ are, respectively, the physical components of $\boldsymbol{v}$ and $\boldsymbol{T}$.

We can also introduce analogous local bases for each point $p \in \mathcal{G}(\mathcal{S},\varepsilon)$. As to the covariant basis, $\{\boldsymbol{g}_1(\vartheta,\psi,\zeta), \boldsymbol{g}_2(\vartheta,\psi,\zeta), \boldsymbol{g}_3(\vartheta,\psi,\zeta)\}$, we have

$$\begin{aligned}
\boldsymbol{g}_1(\vartheta,\psi,\zeta) &:= \frac{\partial \boldsymbol{p}}{\partial\vartheta}(\vartheta,\psi,\zeta) = \left(1+\frac{\zeta}{\rho_o}\right)\boldsymbol{e}_1(\vartheta,\psi),\\
\boldsymbol{g}_2(\vartheta,\psi,\zeta) &:= \frac{\partial \boldsymbol{p}}{\partial\psi}(\vartheta,\psi,\zeta) = \left(1+\frac{\zeta}{\rho_o}\right)\boldsymbol{e}_2(\vartheta,\psi),\\
\boldsymbol{g}_3(\vartheta,\psi,\zeta) &:= \boldsymbol{n}(\vartheta,\psi);
\end{aligned}$$

the contravariant basis is $\{\boldsymbol{g}^1(x,\zeta), \boldsymbol{g}^2(x,\zeta), \boldsymbol{g}^3(x,\zeta)\}$, where

$$\begin{aligned}
\boldsymbol{g}^1(x,\zeta) &:= \nabla\vartheta(x,\zeta) = \left(1+\frac{\zeta}{\rho_o}\right)^{-1}\boldsymbol{e}^1(x),\\
\boldsymbol{g}^2(x,\zeta) &:= \nabla\psi(x,\zeta) = \left(1+\frac{\zeta}{\rho_o}\right)^{-1}\boldsymbol{e}^2(x),\\
\boldsymbol{g}^3(x,\zeta) &:= \boldsymbol{n}(x);
\end{aligned}$$

finally, the physical basis is $\{\boldsymbol{g}_{<1>}(\vartheta,\psi,\zeta), \boldsymbol{g}_{<2>}(\vartheta,\psi,\zeta), \boldsymbol{g}_{<3>}(\vartheta,\psi,\zeta)\}$, where

$$\begin{aligned}
\boldsymbol{g}_{<1>}(\vartheta,\psi,\zeta) &:= \frac{\boldsymbol{g}_1(\vartheta,\psi,\zeta)}{|\boldsymbol{g}_1(\vartheta,\psi,\zeta)|} = \frac{\boldsymbol{g}^1(p(\vartheta,\psi,\zeta))}{|\boldsymbol{g}^1(p(\vartheta,\psi,\zeta))|} = \boldsymbol{e}_{<1>}(\vartheta,\psi) = \cos\vartheta\,\boldsymbol{c}(\psi) - \sin\vartheta\,\boldsymbol{c}_3,\\
\boldsymbol{g}_{<2>}(\vartheta,\psi,\zeta) &:= \frac{\boldsymbol{g}_2(\vartheta,\psi,\zeta)}{|\boldsymbol{g}_2(\vartheta,\psi,\zeta)|} = \frac{\boldsymbol{g}^2(p(\vartheta,\psi,\zeta))}{|\boldsymbol{g}^2(p(\vartheta,\psi,\zeta))|} = \boldsymbol{e}_{<2>}(\vartheta,\psi) = \boldsymbol{c}'(\psi),\\
\boldsymbol{g}_{<3>}(\vartheta,\psi,\zeta) &:= \boldsymbol{n}(\vartheta,\psi) = \sin\vartheta\,\boldsymbol{c}(\psi) + \cos\vartheta\,\boldsymbol{c}_3;
\end{aligned}$$

hence, the two physical bases at points $x \in \mathcal{S}$ and $p \in \mathcal{G}(\mathcal{S},\varepsilon)$ are equal.

## 2.2 Metric and Shift Tensors. Curvature Tensor

Given the elements of the local bases, we can construct some second-order tensors involving geometric features of shells. We define the two *shift tensors* –

briefly, the *shifters* –

$$\boldsymbol{A}(x,\zeta) := \boldsymbol{g}_i \otimes \boldsymbol{e}^i = {}^{\mathrm{s}}\boldsymbol{A}(x,\zeta) + \boldsymbol{n}(x) \otimes \boldsymbol{n}(x), \quad {}^{\mathrm{s}}\boldsymbol{A}(x,\zeta) := \boldsymbol{g}_\beta \otimes \boldsymbol{e}^\beta;$$
$$\boldsymbol{B}(x,\zeta) := \boldsymbol{g}^i \otimes \boldsymbol{e}_i = {}^{\mathrm{s}}\boldsymbol{B}(x,\zeta) + \boldsymbol{n}(x) \otimes \boldsymbol{n}(x), \quad {}^{\mathrm{s}}\boldsymbol{B}(x,\zeta) := \boldsymbol{g}^\beta \otimes \boldsymbol{e}_\beta.$$

Shifter $\boldsymbol{A}(x,\zeta)$ maps the covariant basis at $x$ into the covariant basis at $p$:

$$\boldsymbol{A}\boldsymbol{e}_k = \boldsymbol{g}_k, \quad k = 1,2,3;$$

the role of $\boldsymbol{B}(x,\zeta)$, relating the two contravariant bases at $x$ and $p$, is completely analogous. It can be shown [18] that the ratio of the volume measures at $p$ and $x$ is equal to the determinant of $\boldsymbol{A}$:

$$dvol(p) = \alpha(x,\zeta)\, dvol(x), \quad \alpha := \det \boldsymbol{A};$$

for a spherical shell, we have

$$\boldsymbol{A}(x,\zeta) = \left(1 + \frac{\zeta}{\rho_o}\right) \boldsymbol{e}_{<\beta>} \otimes \boldsymbol{e}_{<\beta>} + \boldsymbol{n} \otimes \boldsymbol{n}, \quad \alpha(x,\zeta) = \left(1 + \frac{\zeta}{\rho_o}\right)^2.$$

On the other hand, the surface shifter ${}^{\mathrm{s}}\boldsymbol{B}$ enters the expression of the gradient of the fiber-wise constant extension to $\mathcal{G}(\mathcal{S},\varepsilon)$ of a scalar or vector field defined over $\mathcal{S}$. For $\eta$ a scalar field over $\mathcal{S}$, denoting its extension by $\widetilde{\eta}$, we have

$$\nabla\widetilde{\eta} = {}^{\mathrm{s}}\boldsymbol{B}\, {}^{\mathrm{s}}\nabla\eta;$$

whereas, for $\boldsymbol{\eta}$ a vector field over $\mathcal{S}$, analogously we find

$$\nabla\widetilde{\boldsymbol{\eta}} = ({}^{\mathrm{s}}\nabla\boldsymbol{\eta})\, {}^{\mathrm{s}}\boldsymbol{B}^T.$$

From now on, we will not make any notational distinction between a field defined over $\mathcal{S}$ and its fiber-wise constant extension to $\mathcal{G}(\mathcal{S},\varepsilon)$, i.e. we shall write the last two equalities as $\nabla\eta = {}^{\mathrm{s}}\boldsymbol{B}\, {}^{\mathrm{s}}\nabla\eta$ and $\nabla\boldsymbol{\eta} = ({}^{\mathrm{s}}\nabla\boldsymbol{\eta})\, {}^{\mathrm{s}}\boldsymbol{B}^T$, respectively.

We also introduce the *metric tensors*

$$\boldsymbol{P} := \boldsymbol{e}_i \otimes \boldsymbol{e}^i = \boldsymbol{e}^i \otimes \boldsymbol{e}_i = {}^{\mathrm{s}}\boldsymbol{P} + \boldsymbol{n} \otimes \boldsymbol{n}, \quad {}^{\mathrm{s}}\boldsymbol{P} := \boldsymbol{e}_\beta \otimes \boldsymbol{e}^\beta = \boldsymbol{e}^\beta \otimes \boldsymbol{e}_\beta = \boldsymbol{e}_{<\beta>} \otimes \boldsymbol{e}_{<\beta>},$$

$$\boldsymbol{G} := \boldsymbol{g}^i \otimes \boldsymbol{g}_i = \boldsymbol{g}_i \otimes \boldsymbol{g}^i = {}^{\mathrm{s}}\boldsymbol{G} + \boldsymbol{n} \otimes \boldsymbol{n}, \quad {}^{\mathrm{s}}\boldsymbol{G} := \boldsymbol{g}^\beta \otimes \boldsymbol{g}_\beta = \boldsymbol{g}_\beta \otimes \boldsymbol{g}^\beta = \boldsymbol{g}_{<\beta>} \otimes \boldsymbol{g}_{<\beta>}.$$

These symmetric second-order tensors are termed as follows: $\boldsymbol{P}$ (${}^{\mathrm{s}}\boldsymbol{P}$) is the metric tensor (surface metric tensor) at point $x \in \mathcal{S}$; $\boldsymbol{G}$ (${}^{\mathrm{s}}\boldsymbol{G}$) is the metric tensor (surface metric tensor) at point $p \in \mathcal{G}(\mathcal{S}, \varepsilon)$, ${}^{\mathrm{s}}\boldsymbol{G}$ being relative to surface $\mathcal{S}_h$. In the case of a spherical shell, we have $\boldsymbol{G} = \boldsymbol{P}$ (and therefore ${}^{\mathrm{s}}\boldsymbol{G} = {}^{\mathrm{s}}\boldsymbol{P}$).

Finally, we define the *curvature tensor*

$$\boldsymbol{W} := -{}^{\mathrm{s}}\nabla \boldsymbol{n} = -\boldsymbol{n}_{,\beta} \otimes \boldsymbol{e}^\beta;$$

for a spherical shell, we have $\boldsymbol{n} = \rho_o^{-1}\boldsymbol{x}$, hence the curvature tensor is just a multiple of the surface metric tensor relative to $\mathcal{S}$:

$$\boldsymbol{W} = -\frac{1}{\rho_o}\, \boldsymbol{e}_\beta \otimes \boldsymbol{e}^\beta = -\frac{1}{\rho_o}\, {}^{\mathrm{s}}\boldsymbol{P}.$$

Given the previous definitions, the following equalities can be shown to hold:

$$\begin{aligned} \boldsymbol{B}^T\boldsymbol{A} = \boldsymbol{P}, \quad \boldsymbol{A}\boldsymbol{B}^T = \boldsymbol{G}; \\ {}^{\mathrm{s}}\boldsymbol{A}(x, \zeta) = {}^{\mathrm{s}}\boldsymbol{P}(x) - \zeta \boldsymbol{W}(x). \end{aligned} \tag{2.3}$$

# Chapter 3

# Kinematics

## 3.1 Displacement Field

In view of the application we have in mind, we choose the following representation for the displacement field:

$$\begin{aligned}
&\boldsymbol{u}(x,\zeta;t) = \overset{(0)}{\boldsymbol{u}}(x,t) + \zeta \overset{(1)}{\boldsymbol{u}}(x,t),\\
&\overset{(0)}{\boldsymbol{u}}(x,t) = \boldsymbol{a}(x,t) + w(x,t)\boldsymbol{n}(x), \quad \overset{(1)}{\boldsymbol{u}}(x,t) = \boldsymbol{\varphi}(x,t) + \gamma(x,t)\boldsymbol{n}(x), \qquad (3.1)\\
&\boldsymbol{a}(x,t)\cdot\boldsymbol{n}(x) = 0,\ \boldsymbol{\varphi}(x,t)\cdot\boldsymbol{n}(x) = 0, \quad \forall x \in \mathcal{S},\ \forall t \in (0,+\infty),
\end{aligned}$$

where $t$ denotes time. This representation, whose graphic interpretation is provided in Fig. 3.1, does not forbid transverse shear deformations, nor thickness distension. It involves six scalar kinematical parameters; in fact, vector fields $\boldsymbol{a}$ and $\boldsymbol{\varphi}$ are both orthogonal to $\boldsymbol{n}$.

Given the displacement field $\boldsymbol{u}$, its gradient has the following expression:

$$\begin{aligned}
\nabla\boldsymbol{u} = \rho_o^{-1}\left(1+\frac{\zeta}{\rho_o}\right)^{-1} &\left\{\boldsymbol{a}_{,1}\otimes\boldsymbol{g}^{<1>} + (\sin\vartheta)^{-1}\boldsymbol{a}_{,2}\otimes\boldsymbol{g}^{<2>} + \zeta\left(\boldsymbol{\varphi}_{,1}\otimes\boldsymbol{g}^{<1>}+\right.\right.\\
&+ \left.\left.(\sin\vartheta)^{-1}\boldsymbol{\varphi}_{,2}\otimes\boldsymbol{g}^{<2>}\right) + (w_{,1}+\zeta\gamma_{,1})\boldsymbol{n}\otimes\boldsymbol{g}^{<1>} + (\sin\vartheta)^{-1}(w_{,2}+\zeta\gamma_{,2})\boldsymbol{n}\otimes\boldsymbol{g}^{<2>}+\right.\\
&+ \left.(w+\zeta\gamma)(\boldsymbol{g}^{<1>}\otimes\boldsymbol{g}^{<1>} + \boldsymbol{g}^{<2>}\otimes\boldsymbol{g}^{<2>})\right\} + \boldsymbol{\varphi}\otimes\boldsymbol{n} + \gamma\,\boldsymbol{n}\otimes\boldsymbol{n},
\end{aligned}$$

and the *strain tensor* is defined by

$$\boldsymbol{E}(x,\zeta;t) := \operatorname{sym}\nabla\boldsymbol{u}(x,\zeta;t).$$

We record here the physical components of the strain tensor, for later use. They are given by

$$2E_{<ij>} = \nabla\boldsymbol{u}\cdot(\boldsymbol{g}_{<i>}\otimes\boldsymbol{g}_{<j>}+\boldsymbol{g}_{<j>}\otimes\boldsymbol{g}_{<i>}) \quad (i,j=1,2,3);$$

this formula yields the following expressions:

$$\begin{aligned}
E_{<11>} &= \rho_o^{-1}\left(1+\frac{\zeta}{\rho_o}\right)^{-1}\left\{a_{<1>,1}+w+\zeta(\varphi_{<1>,1}+\gamma)\right\},\\
E_{<22>} &= \rho_o^{-1}\left(1+\frac{\zeta}{\rho_o}\right)^{-1}\left\{(\sin\vartheta)^{-1}a_{<2>,2}+\cot\vartheta\, a_{<1>}+w+\right.\\
&\quad \left.+\zeta\left[(\sin\vartheta)^{-1}\varphi_{<2>,2}+\cot\vartheta\,\varphi_{<1>}+\gamma\right]\right\},\\
E_{<33>} &= \gamma,\\
E_{<12>} &= \frac{1}{2}\rho_o^{-1}\left(1+\frac{\zeta}{\rho_o}\right)^{-1}\left\{(\sin\vartheta)^{-1}a_{<1>,2}-\cot\vartheta\, a_{<2>}+a_{<2>,1}+\right.\\
&\quad \left.+\zeta\left[(\sin\vartheta)^{-1}\varphi_{<1>,2}-\cot\vartheta\,\varphi_{<2>}+\varphi_{<2>,1}\right]\right\},\\
E_{<13>} &= \frac{1}{2}\left\{\varphi_{<1>}+\rho_o^{-1}\left(1+\frac{\zeta}{\rho_o}\right)^{-1}\left[w_{,1}-a_{<1>}+\zeta(\gamma_{,1}-\varphi_{<1>})\right]\right\},\\
E_{<23>} &= \frac{1}{2}\left\{\varphi_{<2>}+\rho_o^{-1}\left(1+\frac{\zeta}{\rho_o}\right)^{-1}\left[(\sin\vartheta)^{-1}w_{,2}-a_{<2>}+\zeta\left((\sin\vartheta)^{-1}\gamma_{,2}-\varphi_{<2>}\right)\right]\right\}.
\end{aligned} \tag{3.2}$$

**Remark 2.** The motion of the typical material fiber $\mathcal{F}(x)$ can be split into its *rigid* part, characterized by a displacement field $\boldsymbol{u}_{rig}$, and its *strain* part, characterized by $\boldsymbol{u}_{str}$:

$$\boldsymbol{u} = \boldsymbol{u}_{rig}+\boldsymbol{u}_{str}.$$

It is immediate to recognize that $\boldsymbol{u}_{str} = \zeta\gamma\boldsymbol{n}$; furthermore, we can write

$$\boldsymbol{u}_{rig} = \boldsymbol{u}_t+\boldsymbol{u}_r,$$

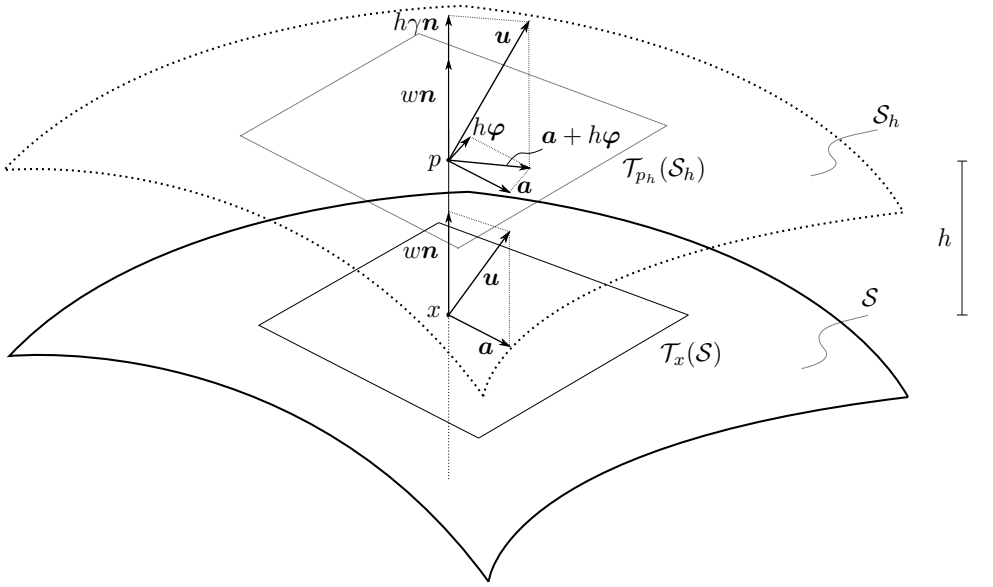


Figure 3.1: Displacement field and its parameters, for a shell-like region modeled over a general middle surface $\mathcal{S}$.

where $\boldsymbol{u}_t$ characterizes translation and $\boldsymbol{u}_r$ rotation. Introducing the *rotation vector* $\boldsymbol{\omega} := \boldsymbol{n} \times \boldsymbol{\varphi}$, we have, respectively,

$$\boldsymbol{u}_t = \boldsymbol{a} + w\boldsymbol{n}, \quad \boldsymbol{u}_r = \zeta\boldsymbol{\varphi} = \boldsymbol{\omega} \times \zeta\boldsymbol{n} = \boldsymbol{\omega} \times (p - x).$$

In fact, it is straightforward to note that

$$\boldsymbol{n} \times \boldsymbol{\omega} = \boldsymbol{n} \times (\boldsymbol{n} \times \boldsymbol{\varphi}) = -\boldsymbol{\varphi},$$

whence $\boldsymbol{\varphi} = \boldsymbol{\omega} \times \boldsymbol{n}$. Therefore, vector $\boldsymbol{\varphi}$ does *not* represent the rotation vector of $\mathcal{F}(x)$.

There are two known representation formulae for the displacement field of a shell-like body, *Reissner-Mindlin*'s and *Kirchhoff-Love*'s; (3.1) is more general than both. Further details about the contents of the following subsections can be found in [17].

### 3.1.1 Reissner-Mindlin's Representation

This representation of the displacement field forbids thickness distension. The corresponding scalar kinematical constraint is

$$\boldsymbol{E} \cdot \boldsymbol{n} \otimes \boldsymbol{n} \equiv 0,$$

which, in terms of the parameters of (3.1), reads

$$\gamma \equiv 0.$$

Thus, $\overset{(1)}{\boldsymbol{u}} = \boldsymbol{\varphi}$ and we get Reissner-Mindlin's displacement field

$$\boldsymbol{u}_{RM}(x, \zeta; t) = \boldsymbol{a}(x, t) + w(x, t)\boldsymbol{n}(x) + \zeta\boldsymbol{\varphi}(x, t);$$

the number of independent scalar parameters is then reduced to five. The motion undergone by $\mathcal{F}(x)$ is completely rigid: it consists of a translation, given by $\boldsymbol{a} + w\boldsymbol{n}$, and a rotation, given by $\boldsymbol{n} \times \boldsymbol{\varphi}$.

### 3.1.2 Kirchhoff-Love's Representation

This representation forbids both thickness distension and transverse shear deformations. The corresponding scalar kinematical constraints are, respectively,

$$\begin{aligned} &\boldsymbol{E} \cdot \boldsymbol{n} \otimes \boldsymbol{n} \equiv 0, \\ &\boldsymbol{E} \cdot \boldsymbol{g}_\beta \otimes \boldsymbol{n} \equiv 0 \quad (\beta = 1, 2). \end{aligned} \tag{3.3}$$

In terms of the parameters of (3.1), again, $(3.3)_1$ reads

$$\gamma \equiv 0;$$

on the other hand, it can be shown that the two scalar constraints $(3.3)_2$ are equivalent to the vector constraint

$$\boldsymbol{\varphi} + \boldsymbol{W}\boldsymbol{a} + {}^{\mathrm{s}}\nabla w \equiv \mathbf{0}.$$

Again, these constraints modify only the representation of $\overset{(1)}{\boldsymbol{u}}$, which becomes $\overset{(1)}{\boldsymbol{u}} = -\boldsymbol{W}\boldsymbol{a} - {}^{\mathrm{s}}\nabla w$. Moreover, using identity $(2.3)_3$, we can finally get Kirchhoff-Love's representation of the displacement field,

$$\boldsymbol{u}_{KL}(x,\zeta;t) = {}^{\mathrm{s}}\boldsymbol{A}(x,\zeta)\boldsymbol{a}(x,t) + w(x,t)\boldsymbol{n}(x) - \zeta\,{}^{\mathrm{s}}\nabla w(x,t),$$

which involves only three scalar parameters: the two components of $\boldsymbol{a}$ and $w$.

# Chapter 4

# Field Equations

In this chapter, we derive the general balance and evolution equations. We shall not deal with boundary equations, since for spherical shells $\partial\mathcal{S} = \emptyset$. All the fields involved in the following arguments are defined in the referential configuration of the shell under study.

## 4.1 Weak Formulation

Let $\delta\boldsymbol{u}$ be a virtual displacement field of the same form as (3.1), namely,

$$\delta\boldsymbol{u}(x,\zeta;t) = \overset{(0)}{\delta\boldsymbol{u}}(x,t) + \zeta\,\overset{(1)}{\delta\boldsymbol{u}}(x,t).$$

### 4.1.1 Internal Virtual Work

Let $\boldsymbol{S}$ be the Piola stress tensor [19]. The expenditure of *internal virtual work* over the shell-like body $\mathcal{G} = \mathcal{G}(\mathcal{S},\varepsilon)$ is

$$\mathcal{W}^{int}(\mathcal{G})\,[\delta\boldsymbol{u}] := \int_{\mathcal{G}} \boldsymbol{S}\cdot\nabla\delta\boldsymbol{u}.$$

Following the same procedure used in [7] and calculating

$$
\begin{aligned}
{}^{\mathrm{s}}\nabla \overset{(0)}{\delta \boldsymbol{u}} &= {}^{\mathrm{s}}\nabla \delta \boldsymbol{a} + \boldsymbol{n} \otimes {}^{\mathrm{s}}\nabla \delta w + \delta w \, {}^{\mathrm{s}}\nabla \boldsymbol{n}, \\
{}^{\mathrm{s}}\nabla \overset{(1)}{\delta \boldsymbol{u}} &= {}^{\mathrm{s}}\nabla \delta \boldsymbol{\varphi} + \boldsymbol{n} \otimes {}^{\mathrm{s}}\nabla \delta \gamma + \delta \gamma \, {}^{\mathrm{s}}\nabla \boldsymbol{n},
\end{aligned}
$$

the internal virtual work takes the form

$$
\begin{aligned}
\mathcal{W}^{int}(\mathcal{G})\left[\delta \boldsymbol{a}, \delta w, \delta \boldsymbol{\varphi}, \delta \gamma\right] = \int_{\mathcal{S}} \big\{ & {}^{\mathrm{s}}\boldsymbol{F} \cdot {}^{\mathrm{s}}\nabla \delta \boldsymbol{a} + {}^{\mathrm{s}}\boldsymbol{M} \cdot {}^{\mathrm{s}}\nabla \delta \boldsymbol{\varphi} + {}^{\mathrm{s}}\boldsymbol{F}^{T}\boldsymbol{n} \cdot {}^{\mathrm{s}}\nabla \delta w + \\
& + {}^{\mathrm{s}}\boldsymbol{M}^{T}\boldsymbol{n} \cdot {}^{\mathrm{s}}\nabla \delta \gamma + \left({}^{\mathrm{s}}\boldsymbol{F} \cdot {}^{\mathrm{s}}\nabla \boldsymbol{n}\right) \delta w + \\
& + \left( \boldsymbol{f}^{(3)} \cdot \boldsymbol{n} + {}^{\mathrm{s}}\boldsymbol{M} \cdot {}^{\mathrm{s}}\nabla \boldsymbol{n} \right) \delta \gamma + \boldsymbol{f}^{(3)} \cdot \delta \boldsymbol{\varphi} \big\},
\end{aligned}
\tag{4.1}
$$

where

$$
\begin{aligned}
{}^{\mathrm{s}}\boldsymbol{F}(x,t) &:= \int_{I} \alpha(x,\zeta) \boldsymbol{S}(x,\zeta;t) \, {}^{\mathrm{s}}\boldsymbol{B}(x,\zeta) \, d\zeta = \left( \int_{I} \alpha \boldsymbol{S}\boldsymbol{g}^{\beta} \, d\zeta \right) \otimes \boldsymbol{e}_{\beta}, \\
{}^{\mathrm{s}}\boldsymbol{M}(x,t) &:= \int_{I} \alpha(x,\zeta) \zeta \boldsymbol{S}(x,\zeta;t) \, {}^{\mathrm{s}}\boldsymbol{B}(x,\zeta) \, d\zeta = \left( \int_{I} \alpha \zeta \boldsymbol{S}\boldsymbol{g}^{\beta} \, d\zeta \right) \otimes \boldsymbol{e}_{\beta}, \\
\boldsymbol{f}^{(3)}(x,t) &:= \int_{I} \alpha(x,\zeta) \boldsymbol{S}(x,\zeta;t) \boldsymbol{n}(x) \, d\zeta.
\end{aligned}
\tag{4.2}
$$

We call ${}^{\mathrm{s}}\boldsymbol{F}$ the *force tensor*, ${}^{\mathrm{s}}\boldsymbol{M}$ the *moment tensor* and $\boldsymbol{f}^{(3)}$ the *shear vector*.

### 4.1.2 External Virtual Work

The system of external loads is made of:

- the *distance force* per unit volume $\boldsymbol{d}_o = \boldsymbol{d}_o^{mi} + \boldsymbol{d}_o^{in}$, the former addend being its *non-inertial* part, the latter its *inertial* part. Denoting the mass density of the shell by $\delta_o$, we have

$$
\boldsymbol{d}_o^{in}(x,\zeta;t) = -\delta_o \ddot{\boldsymbol{u}}(x,\zeta;t);
$$

- the *contact force* $\boldsymbol{c}_o$ per unit area, acting on the boundary $\partial\mathcal{G}$ of the shell.

We write $\partial\mathcal{G} = \mathcal{S}^- \cup \mathcal{S}^+$, where $\mathcal{S}^\pm := \{x \pm \varepsilon \boldsymbol{n}(x) : x \in \mathcal{S}\}$, and use the notation

$$\Psi^\pm(x) := \Psi(x, \pm\varepsilon)$$

for the restriction of a field $\Psi$ to $\mathcal{S}^\pm$.

The expenditure of *external virtual work* over the shell-like body is

$$\mathcal{W}^{ext}(\mathcal{G})\,[\delta\boldsymbol{u}] := \int_{\mathcal{G}} \boldsymbol{d}_o \cdot \delta\boldsymbol{u} + \int_{\partial\mathcal{G}} \boldsymbol{c}_o \cdot \delta\boldsymbol{u}.$$

Again, choosing $\delta\boldsymbol{u}$ of the same form as (3.1) and following the same procedure set forth in [7], we get

$$\mathcal{W}^{ext}(\mathcal{G})\,[\delta\boldsymbol{a}, \delta w, \delta\boldsymbol{\varphi}, \delta\gamma] = \int_{\mathcal{S}} \left\{\boldsymbol{q}_o \cdot \delta\boldsymbol{a} + (\boldsymbol{q}_o \cdot \boldsymbol{n})\delta w + \boldsymbol{r}_o \cdot \delta\boldsymbol{\varphi} + (\boldsymbol{r}_o \cdot \boldsymbol{n})\delta\gamma\right\}, \tag{4.3}$$

where

$$\begin{aligned} \boldsymbol{q}_o(x,t) &:= \int_I \alpha(x,\zeta)\, \boldsymbol{d}_o(x,\zeta;t)\, d\zeta + \alpha^+(x)\boldsymbol{c}_o^+(x) + \alpha^-(x)\boldsymbol{c}_o^-(x), \\ \boldsymbol{r}_o(x,t) &:= \int_I \alpha(x,\zeta)\zeta \boldsymbol{d}_o(x,\zeta;t)\, d\zeta + \varepsilon\left(\alpha^+(x)\boldsymbol{c}_o^+(x) - \alpha^-(x)\boldsymbol{c}_o^-(x)\right) \end{aligned} \tag{4.4}$$

are the *distance force* and the *distance couple* per unit area, respectively. The decomposition $\boldsymbol{d}_o = \boldsymbol{d}_o^{in} + \boldsymbol{d}_o^{ni}$ implies analogous decompositions for $\boldsymbol{q}_o$ and $\boldsymbol{r}_o$: $\boldsymbol{q}_o = \boldsymbol{q}_o^{in} + \boldsymbol{q}_o^{ni}$, $\boldsymbol{r}_o = \boldsymbol{r}_o^{in} + \boldsymbol{r}_o^{ni}$; in particular, we find that

$$\begin{aligned} \boldsymbol{q}_o^{in}(x,t) &= \int_I \alpha(x,\zeta)\, \boldsymbol{d}_o^{in}(x,\zeta;t)\, d\zeta = -2\varepsilon\delta_o \left\{\left(1 + \frac{\varepsilon^2}{3\rho_o^2}\right)\frac{\partial^2 \overset{(0)}{\boldsymbol{u}}}{\partial t^2}(x,t) + \frac{2\varepsilon^2}{3\rho_o}\frac{\partial^2 \overset{(1)}{\boldsymbol{u}}}{\partial t^2}(x,t)\right\}, \\ \boldsymbol{r}_o^{in}(x,t) &= \int_I \alpha(x,\zeta)\zeta \boldsymbol{d}_o^{in}(x,\zeta;t)\, d\zeta = -2\varepsilon^3\delta_o \left\{\frac{2}{3\rho_o}\frac{\partial^2 \overset{(0)}{\boldsymbol{u}}}{\partial t^2}(x,t) + \left(\frac{1}{3} + \frac{\varepsilon^2}{5\rho_o^2}\right)\frac{\partial^2 \overset{(1)}{\boldsymbol{u}}}{\partial t^2}(x,t)\right\}. \end{aligned} \tag{4.5}$$

### 4.1.3 Principle of Virtual Work

All in all, the weak formulation of the equilibrium problem (*Principle of Virtual Work*) reads:

$$\forall \delta\boldsymbol{a}, \delta w, \delta\boldsymbol{\varphi}, \delta\gamma, \quad \mathcal{W}^{ext}(\mathcal{G})\left[\delta\boldsymbol{a}, \delta w, \delta\boldsymbol{\varphi}, \delta\gamma\right] = \mathcal{W}^{int}(\mathcal{G})\left[\delta\boldsymbol{a}, \delta w, \delta\boldsymbol{\varphi}, \delta\gamma\right],$$

that is to say,

$$\begin{aligned}
&\int_{\mathcal{S}} \{\boldsymbol{q}_o \cdot \delta\boldsymbol{a} + (\boldsymbol{q}_o \cdot \boldsymbol{n})\delta w \, + \boldsymbol{r}_o \cdot \delta\boldsymbol{\varphi} + (\boldsymbol{r}_o \cdot \boldsymbol{n})\delta\gamma\} = \\
&\int_{\mathcal{S}} \big\{ {}^{\mathrm{s}}\boldsymbol{F} \cdot {}^{\mathrm{s}}\nabla\delta\boldsymbol{a} + {}^{\mathrm{s}}\boldsymbol{M} \cdot {}^{\mathrm{s}}\nabla\delta\boldsymbol{\varphi} + {}^{\mathrm{s}}\boldsymbol{F}^T\boldsymbol{n} \cdot {}^{\mathrm{s}}\nabla\delta w + \\
&\quad + {}^{\mathrm{s}}\boldsymbol{M}^T\boldsymbol{n} \cdot {}^{\mathrm{s}}\nabla\delta\gamma + ({}^{\mathrm{s}}\boldsymbol{F} \cdot {}^{\mathrm{s}}\nabla\boldsymbol{n})\, \delta w + \\
&+ \left(\boldsymbol{f}^{(3)} \cdot \boldsymbol{n} + {}^{\mathrm{s}}\boldsymbol{M} \cdot {}^{\mathrm{s}}\nabla\boldsymbol{n}\right) \delta\gamma + \boldsymbol{f}^{(3)} \cdot \delta\boldsymbol{\varphi} \big\}.
\end{aligned} \tag{4.6}$$

## 4.2 Balance Equations

The weak formulation (4.6) can be rewritten, by integration by parts, as follows:

$$\int_{\mathcal{S}} \left\{ (-{}^{\mathrm{s}}\mathrm{Div}\, {}^{\mathrm{s}}\boldsymbol{F} - \boldsymbol{q}_o) \cdot (\delta\boldsymbol{a} + \delta w\boldsymbol{n}) + (-{}^{\mathrm{s}}\mathrm{Div}\, {}^{\mathrm{s}}\boldsymbol{M} + \boldsymbol{f}^{(3)} - \boldsymbol{r}_o) \cdot (\delta\boldsymbol{\varphi} + \delta\gamma\boldsymbol{n}) \right\} = 0, \tag{4.7}$$

whence, by localization, the following point-wise balance equations have to be satisfied in $\mathcal{S}$:

$$\begin{aligned}
&{}^{\mathrm{s}}\mathrm{Div}\, {}^{\mathrm{s}}\boldsymbol{F} + \boldsymbol{q}_o = \boldsymbol{0}, \\
&{}^{\mathrm{s}}\mathrm{Div}\, {}^{\mathrm{s}}\boldsymbol{M} - \boldsymbol{f}^{(3)} + \boldsymbol{r}_o = \boldsymbol{0}.
\end{aligned} \tag{4.8}$$

To provide a component-wise version of these equations, we first define

$$\begin{aligned}
&\boldsymbol{F} := {}^{\mathrm{s}}\boldsymbol{F} + \boldsymbol{f}^{(3)} \otimes \boldsymbol{n} = \left( \int_I \alpha \boldsymbol{S}\boldsymbol{g}^i \, d\zeta \right) \otimes \boldsymbol{e}_i, \\
&\boldsymbol{M} := {}^{\mathrm{s}}\boldsymbol{M} + \boldsymbol{m}^{(3)} \otimes \boldsymbol{n} = \left( \int_I \alpha\zeta \boldsymbol{S}\boldsymbol{g}^i \, d\zeta \right) \otimes \boldsymbol{e}_i, \quad \boldsymbol{m}^{(3)} := \int_I \alpha\zeta \boldsymbol{S}\boldsymbol{n} \, d\zeta
\end{aligned} \tag{4.9}$$

We call *membrane forces* the contravariant components $F^{\alpha\beta} := \boldsymbol{F} \cdot \boldsymbol{e}^\alpha \otimes \boldsymbol{e}^\beta = {}^{\mathrm{s}}\boldsymbol{F} \cdot \boldsymbol{e}^\alpha \otimes \boldsymbol{e}^\beta$, *normal membrane forces* for $\alpha = \beta$, *shear membrane forces* for $\alpha \neq \beta$; and we call $M^{\alpha\alpha} := \boldsymbol{M} \cdot \boldsymbol{e}^\alpha \otimes \boldsymbol{e}^\alpha = {}^{\mathrm{s}}\boldsymbol{M} \cdot \boldsymbol{e}^\alpha \otimes \boldsymbol{e}^\alpha$ $(\alpha = 1, 2)$ the *bending moments* and $M^{\alpha\beta} := \boldsymbol{M} \cdot \boldsymbol{e}^\alpha \otimes \boldsymbol{e}^\beta = {}^{\mathrm{s}}\boldsymbol{M} \cdot \boldsymbol{e}^\alpha \otimes \boldsymbol{e}^\beta$ $(\alpha, \beta = 1, 2;\ \alpha \neq \beta)$ the *twisting moments*. Finally, we call $F^{3\alpha} := \boldsymbol{f}^{(3)} \cdot \boldsymbol{e}^\alpha$ the *transverse shears* and $M^{3\alpha} := \boldsymbol{m}^{(3)} \cdot \boldsymbol{e}^\alpha$ the *thickness moments*.

It can be shown that the following system of six scalar equations, involving the physical components of the tensor fields defined in (4.9), is equivalent to the vector equations (4.8):

$$
\begin{aligned}
&(\sin\vartheta\ F_{<11>})_{,1} + F_{<12>,2} - \cos\vartheta\ F_{<22>} + \sin\vartheta\ F_{<31>} + \rho_o \sin\vartheta\ q_{o<1>} = 0,\\
&(\sin\vartheta\ F_{<12>})_{,1} + F_{<22>,2} + \cos\vartheta\ F_{<12>} + \sin\vartheta\ F_{<32>} + \rho_o \sin\vartheta\ q_{o<2>} = 0,\\
&(\sin\vartheta\ F_{<31>})_{,1} + F_{<32>,2} - \sin\vartheta\,(F_{<11>} + F_{<22>} - \rho_o\, q_{o<3>}) = 0,\\
&(\sin\vartheta\ M_{<11>})_{,1} + M_{<12>,2} - \cos\vartheta\ M_{<22>} - \rho_o \sin\vartheta\ F_{<31>} + \rho_o \sin\vartheta\ r_{o<1>} = 0,\\
&(\sin\vartheta\ M_{<12>})_{,1} + M_{<22>,2} + \cos\vartheta\ M_{<12>} - \rho_o \sin\vartheta\ F_{<32>} + \rho_o \sin\vartheta\ r_{o<2>} = 0,\\
&(\sin\vartheta\ M_{<31>})_{,1} + M_{<32>,2} - \sin\vartheta\,(M_{<11>} + M_{<22>} + \rho_o\, F_{<33>} - \rho_o\, r_{o<3>}) = 0.
\end{aligned}
\tag{4.10}
$$

## 4.3 Constitutive Assumptions

For the shell under study, we consider a linearly elastic response of the following kind: *transversely isotropic* at any point with respect to the direction of $\boldsymbol{n}$. Consider the orthonormal basis for the linear space Sym, given by the following tensors:

$$
\begin{aligned}
&\boldsymbol{V}_\beta = \frac{1}{\sqrt{2}}\left(\boldsymbol{g}_{<\beta>} \otimes \boldsymbol{n} + \boldsymbol{n} \otimes \boldsymbol{g}_{<\beta>}\right)\ (\beta = 1, 2), \quad \boldsymbol{V}_3 = \boldsymbol{n} \otimes \boldsymbol{n},\\
&\boldsymbol{W}_\beta = \boldsymbol{g}_{<\beta>} \otimes \boldsymbol{g}_{<\beta>}\ (\beta \text{ not summed}),\ \boldsymbol{W}_3 = \frac{1}{\sqrt{2}}\left(\boldsymbol{g}_{<1>} \otimes \boldsymbol{g}_{<2>} + \boldsymbol{g}_{<2>} \otimes \boldsymbol{g}_{<1>}\right).
\end{aligned}
\tag{4.11}
$$

Given this basis, a representation formula for the elasticity tensor reflecting our constitutive assumption can be found in [18]; five independent elastic moduli

are involved in this representation. However, in technical applications, these quantities are replaced by six technical moduli – two Young-like, three Poisson-like and one shear-like – that must satisfy an algebraic condition. The technical moduli, which we assume to vary with point $x \in \mathcal{S}$, enter the representation of the *compliance tensor*, i.e., the inverse of the elasticity tensor $\mathbb{C}$, as follows[1]:

$$\begin{aligned}\mathbb{C}^{-1} = &\frac{1}{E_p}\left(\boldsymbol{W}_1 \otimes \boldsymbol{W}_1 + \boldsymbol{W}_2 \otimes \boldsymbol{W}_2\right) + \frac{1}{E_n}\boldsymbol{V}_3 \otimes \boldsymbol{V}_3 + \\ &- \frac{\nu_p}{E_p}\left(\boldsymbol{W}_1 \otimes \boldsymbol{W}_2 + \boldsymbol{W}_2 \otimes \boldsymbol{W}_1\right) - \frac{\nu_{pn}}{E_p}\left(\boldsymbol{V}_3 \otimes \boldsymbol{W}_1 + \boldsymbol{V}_3 \otimes \boldsymbol{W}_2\right) + \\ &- \frac{\nu_{np}}{E_n}\left(\boldsymbol{W}_1 \otimes \boldsymbol{V}_3 + \boldsymbol{W}_2 \otimes \boldsymbol{V}_3\right) + \frac{1}{2G}\left(\boldsymbol{V}_1 \otimes \boldsymbol{V}_1 + \boldsymbol{V}_2 \otimes \boldsymbol{V}_2\right) + \\ &+ \frac{1+\nu_p}{E_p}\boldsymbol{W}_3 \otimes \boldsymbol{W}_3.\end{aligned} \tag{4.12}$$

Due to the built-in symmetries of $\mathbb{C}$, it results that

$$\frac{E_p}{E_n} = \frac{\nu_{pn}}{\nu_{np}}.$$

In order to understand the mechanical meaning of the technical moduli, we preliminarily fix an arbitrary unit vector $\boldsymbol{e}$ such that $\boldsymbol{e} \cdot \boldsymbol{n} = 0$, and an arbitrary unit vector $\boldsymbol{s}$ such that $\boldsymbol{s} \cdot \boldsymbol{n} = 0$ and $\boldsymbol{s} \cdot \boldsymbol{e} = 0$.

First, consider an uniaxial stress in the direction $\boldsymbol{e}$ induced in a specimen made of the material under examination: $\boldsymbol{S} = \sigma \boldsymbol{e} \otimes \boldsymbol{e}$. Then, the corresponding strain is $\boldsymbol{E} = \mathbb{C}^{-1}[\boldsymbol{S}]$ and we find that the ratio between the axial stress and the axial strain is the *in-plane Young's modulus*

$$E_p = \frac{\boldsymbol{S} \cdot \boldsymbol{e} \otimes \boldsymbol{e}}{\boldsymbol{E} \cdot \boldsymbol{e} \otimes \boldsymbol{e}};$$

moreover, we find the *in-plane* and *first transverse Poisson's moduli*, respectively given by

$$\nu_p = -\frac{\boldsymbol{E} \cdot \boldsymbol{s} \otimes \boldsymbol{s}}{\boldsymbol{E} \cdot \boldsymbol{e} \otimes \boldsymbol{e}}, \quad \nu_{pn} = -\frac{\boldsymbol{E} \cdot \boldsymbol{n} \otimes \boldsymbol{n}}{\boldsymbol{E} \cdot \boldsymbol{e} \otimes \boldsymbol{e}}.$$

[1] Here and in the sequel, we will left tacit the dependence on $x$ of the elasticity and compliance tensors, as well as of the technical moduli.

Now, consider an uniaxial stress in the direction $\boldsymbol{n}$, $\boldsymbol{S} = \sigma \boldsymbol{n} \otimes \boldsymbol{n}$. Analogously, given the corresponding strain $\boldsymbol{E}$, we find the *transverse Young's modulus* and the *second transverse Poisson's modulus*:

$$E_n = \frac{\boldsymbol{S} \cdot \boldsymbol{n} \otimes \boldsymbol{n}}{\boldsymbol{E} \cdot \boldsymbol{n} \otimes \boldsymbol{n}}, \quad \nu_{np} = -\frac{\boldsymbol{E} \cdot \boldsymbol{e} \otimes \boldsymbol{e}}{\boldsymbol{E} \cdot \boldsymbol{n} \otimes \boldsymbol{n}}.$$

Finally, consider a shear stress of the form $\boldsymbol{S} = \tau(\boldsymbol{e} \otimes \boldsymbol{n} + \boldsymbol{n} \otimes \boldsymbol{e})$ and the corresponding strain $\boldsymbol{E}$. Then, we find the *transverse shear modulus*, given by

$$2G = \frac{\boldsymbol{S} \cdot \boldsymbol{e} \otimes \boldsymbol{n}}{\boldsymbol{E} \cdot \boldsymbol{e} \otimes \boldsymbol{n}}.$$

The elasticity tensor can be represented, in terms of the technical moduli, by inversion of (4.12); it results

$$\begin{aligned}
\mathbb{C} =& \frac{E_p}{\Delta} \left[ (1 - \nu_{pn}\nu_{np}) \left( \boldsymbol{W}_1 \otimes \boldsymbol{W}_1 + \boldsymbol{W}_2 \otimes \boldsymbol{W}_2 \right) + \right. \\
&+ (\nu_p + \nu_{pn}\nu_{np}) \left( \boldsymbol{W}_1 \otimes \boldsymbol{W}_2 + \boldsymbol{W}_2 \otimes \boldsymbol{W}_1 \right) + \\
&+ (1 + \nu_p)\nu_{np} \boldsymbol{W}_1 \otimes \boldsymbol{V}_3 + (1 + \nu_p)\nu_{pn} \boldsymbol{W}_2 \otimes \boldsymbol{W}_3 ] + \\
&+ \frac{E_n}{\Delta} \left[ (1 + \nu_p)\nu_{pn} \left( \boldsymbol{V}_3 \otimes \boldsymbol{W}_1 + \boldsymbol{V}_3 \otimes \boldsymbol{W}_2 \right) + \right. \\
&+ \left. (1 - \nu_p^2) \boldsymbol{V}_3 \otimes \boldsymbol{V}_3 \right] + 2G \left( \boldsymbol{V}_1 \otimes \boldsymbol{V}_1 + \boldsymbol{V}_2 \otimes \boldsymbol{V}_2 \right) + \\
&+ \frac{E_p}{1 + \nu_p} \boldsymbol{W}_3 \otimes \boldsymbol{W}_3,
\end{aligned} \tag{4.13}$$

where

$$\Delta := (1 + \nu_p)(1 - \nu_p - 2\nu_{pn}\nu_{np}).$$

Component-wise, the constitutive law $\boldsymbol{S} = \mathbb{C}[\boldsymbol{E}]$, with $\mathbb{C}$ as in (4.13), reads

$$
\begin{aligned}
S_{<11>} &= \frac{E_p}{\Delta}\left[(1-\nu_{pn}\nu_{np})E_{<11>} + (\nu_p+\nu_{pn}\nu_{np})E_{<22>} + (1+\nu_p)\nu_{np}E_{<33>}\right],\\
S_{<22>} &= \frac{E_p}{\Delta}\left[(\nu_p+\nu_{pn}\nu_{np})E_{<11>} + (1-\nu_{pn}\nu_{np})E_{<22>} + (1+\nu_p)\nu_{np}E_{<33>}\right],\\
S_{<33>} &= \frac{E_n}{\Delta}\left[(1+\nu_p)\nu_{pn}(E_{<11>}+E_{<22>}) + (1-\nu_p^2)E_{<33>}\right],\\
S_{<12>} &= \frac{E_p}{1+\nu_p}E_{<12>},\\
S_{<13>} &= 2G\,E_{<13>},\\
S_{<23>} &= 2G\,E_{<23>},
\end{aligned}
\tag{4.14}
$$

where the components $E_{<ij>}$ are expressed as in (3.2). Inserting these relations into the scalar consequences of definitions (4.9), we find:

$$
\begin{aligned}
F_{<11>} = \int_I \left(1+\frac{\zeta}{\rho_o}\right) S_{<11>}\,d\zeta = \frac{2\varepsilon}{\rho_o \sin\vartheta}\frac{E_p}{\Delta}\{&(1-\nu_{pn}\nu_{np})\sin\vartheta(a_{<1>,1}+w)+\\
&+(\nu_p+\nu_{pn}\nu_{np})(\sin\vartheta\, w + a_{<2>,2} + \cos\vartheta\, a_{<1>}) + (1+\nu_p)\nu_{np}\rho_o\sin\vartheta\,\gamma\},
\end{aligned}
\tag{4.15}
$$

$$
\begin{aligned}
F_{<22>} = \int_I \left(1+\frac{\zeta}{\rho_o}\right) S_{<22>}\,d\zeta = \frac{2\varepsilon}{\rho_o \sin\vartheta}\frac{E_p}{\Delta}\{&(\nu_p+\nu_{pn}\nu_{np})\sin\vartheta(a_{<1>,1}+w)+\\
&+(1-\nu_{pn}\nu_{np})(\sin\vartheta\, w + a_{<2>,2} + \cos\vartheta\, a_{<1>}) + (1+\nu_p)\nu_{np}\rho_o\sin\vartheta\,\gamma\},
\end{aligned}
\tag{4.16}
$$

$$
\begin{aligned}
F_{<33>} = \int_I \left(1+\frac{\zeta}{\rho_o}\right)^2 S_{<33>}\,d\zeta = \frac{2\varepsilon}{\rho_o \sin\vartheta}\frac{E_n}{\Delta}\{&(1+\nu_p)\nu_{pn}\,[\sin\vartheta\,(a_{<1>,1}+w+\\
&+\frac{\varepsilon^2}{3\rho_o}(\varphi_{<1>,1}+\gamma)) + a_{<2>,2} + \cos\vartheta\, a_{<1>} + \sin\vartheta\, w+\\
&+\frac{\varepsilon^2}{3\rho_o}(\varphi_{<2>,2} + \cos\vartheta\,\varphi_{<1>} + \sin\vartheta\,\gamma)] + (1-\nu_p^2)\left(1+\frac{\varepsilon^2}{3\rho_o^2}\right)\rho_o\sin\vartheta\,\gamma\},
\end{aligned}
\tag{4.17}
$$

$$F_{<12>} = F_{<21>} = \int_I \left(1 + \frac{\zeta}{\rho_o}\right) S_{<12>}\, d\zeta = \\ = \frac{\varepsilon E_p}{\rho_o \sin\vartheta (1+\nu_p)} \left(a_{<1>,2} - \cos\vartheta\, a_{<2>} + \sin\vartheta\, a_{<2>,1}\right), \tag{4.18}$$

$$F_{<31>} = \int_I \left(1 + \frac{\zeta}{\rho_o}\right) S_{<31>}\, d\zeta = 2\varepsilon G(\varphi_{<1>} + \rho_o^{-1}(w_{,1} - a_{<1>})), \tag{4.19}$$

$$F_{<32>} = \int_I \left(1 + \frac{\zeta}{\rho_o}\right) S_{<32>}\, d\zeta = \frac{2\varepsilon G}{\sin\vartheta}(\sin\vartheta\, \varphi_{<2>} + \rho_o^{-1}(w_{,2} - \sin\vartheta\, a_{<2>})), \tag{4.20}$$

$$M_{<11>} = \int_I \zeta \left(1 + \frac{\zeta}{\rho_o}\right) S_{<11>}\, d\zeta = \frac{2\varepsilon^3}{3\rho_o}\frac{E_p}{\Delta}[(1 - \nu_{pn}\nu_{np})(\varphi_{<1>,1} + \gamma) + \\ + \frac{\nu_p + \nu_{pn}\nu_{np}}{\sin\vartheta}(\varphi_{<2>,2} + \cos\vartheta\, \varphi_{<1>} + \sin\vartheta\, \gamma) + (1+\nu_p)\nu_{np}\, \gamma], \tag{4.21}$$

$$M_{<22>} = \int_I \zeta \left(1 + \frac{\zeta}{\rho_o}\right) S_{<22>}\, d\zeta = \frac{2\varepsilon^3}{3\rho_o}\frac{E_p}{\Delta}\,[(\nu_p + \nu_{pn}\nu_{np})(\varphi_{<1>,1} + \gamma) + \\ + \frac{1 - \nu_{pn}\nu_{np}}{\sin\vartheta}(\varphi_{<2>,2} + \cos\vartheta\, \varphi_{<1>} + \sin\vartheta\, \gamma) + (1+\nu_p)\nu_{np}\, \gamma], \tag{4.22}$$

$$M_{<12>} = M_{<21>} = \int_I \zeta \left(1 + \frac{\zeta}{\rho_o}\right) S_{<12>}\, d\zeta = \\ = \frac{\varepsilon^3 E_p}{3\rho_o \sin\vartheta (1+\nu_p)} \left(\varphi_{<1>,2} - \cos\vartheta\, \varphi_{<2>} + \sin\vartheta\, \varphi_{<2>,1}\right), \tag{4.23}$$

$$M_{<31>} = \int_I \zeta \left(1 + \frac{\zeta}{\rho_o}\right) S_{<31>}\, d\zeta = \frac{2\varepsilon^3 G}{3\rho_o}\gamma_{,1}\,, \tag{4.24}$$

$$M_{<32>} = \int_I \zeta \left(1 + \frac{\zeta}{\rho_o}\right) S_{<32>}\, d\zeta = \frac{2\varepsilon^3 G}{3\rho_o \sin\vartheta}\gamma_{,2}\,. \tag{4.25}$$

## 4.4 General Evolution Equations

Inserting the constitutive equations obtained in the previous section and the scalar consequences of (4.4) and (4.5) into system (4.10), we get the following six equations in the six unknowns $a_{<1>}, a_{<2>}, \varphi_{<1>}, \varphi_{<2>}, w, \gamma$:

$$\{\frac{2\varepsilon}{\rho_o}\frac{E_p}{\Delta}\,[(1-\nu_{pn}\nu_{np})(a_{<1>,1}+w)\sin\vartheta+(\nu_p+\nu_{pn}\nu_{np})(\sin\vartheta\,w+a_{<2>,2}+$$
$$+\ \cos\vartheta\,a_{<1>})+(1+\nu_p)\nu_{np}\rho_o\sin\vartheta\,\gamma]\}_{,1}+\{\frac{\varepsilon E_p}{\rho_o\sin\vartheta(1+\nu_p)}(a_{<1>,2}-\cos\vartheta\,a_{<2>}+$$
$$+\ \sin\vartheta\,a_{<2>,1}\,)\}_{,2}-\frac{2\varepsilon}{\rho_o}\cot\vartheta\,\frac{E_p}{\Delta}\,\{(\nu_p+\nu_{pn}\nu_{np})\sin\vartheta(a_{<1>,1}+w)+$$
$$+\ (1-\nu_{pn}\nu_{np})(\sin\vartheta\,w+a_{<2>,2}+\cos\vartheta\,a_{<1>})+(1+\nu_p)\nu_{np}\rho_o\sin\vartheta\,\gamma\}+$$
$$+\ 2\varepsilon G\sin\vartheta(\varphi_{<1>}+\rho_o^{-1}(w_{,1}-a_{<1>}))+\rho_o\sin\vartheta\ q_o^{ni}{}_{<1>}=$$
$$=2\varepsilon\rho_o\delta_o\sin\vartheta\left\{\left(1+\frac{\varepsilon^2}{3\rho_o^2}\right)\ddot{a}_{<1>}+\frac{2\varepsilon^2}{3\rho_o}\ddot{\varphi}_{<1>}\right\},\tag{4.26}$$

$$\left\{\frac{\varepsilon E_p}{\rho_o(1+\nu_p)}\,(a_{<1>,2}-\cos\vartheta\,a_{<2>}+\sin\vartheta\,a_{<2>,1}\,)\right\}_{,1}+$$
$$+\ \{\frac{2\varepsilon}{\rho_o\sin\vartheta}\frac{E_p}{\Delta}\,[(\nu_p+\nu_{pn}\nu_{np})\sin\vartheta(a_{<1>,1}+w)+$$
$$+\ (1-\nu_{pn}\nu_{np})(\sin\vartheta\,w+a_{<2>,2}+\cos\vartheta\,a_{<1>})+(1+\nu_p)\nu_{np}\rho_o\sin\vartheta\,\gamma]\}_{,2}+$$
$$+\ \frac{\varepsilon E_p\cot\vartheta}{\rho_o(1+\nu_p)}\,(a_{<1>,2}-\cos\vartheta\,a_{<2>}+\sin\vartheta\,a_{<2>,1}\,)+$$
$$+\ 2\varepsilon G(\sin\vartheta\,\varphi_{<2>}+\rho_o^{-1}(w_{,2}-\sin\vartheta\,a_{<2>}))+\rho_o\sin\vartheta\ q_o^{ni}{}_{<2>}=$$
$$=2\varepsilon\rho_o\delta_o\sin\vartheta\left\{\left(1+\frac{\varepsilon^2}{3\rho_o^2}\right)\ddot{a}_{<2>}+\frac{2\varepsilon^2}{3\rho_o}\ddot{\varphi}_{<2>}\right\},\tag{4.27}$$

$$\left\{2\varepsilon G\sin\vartheta(\varphi_{<1>}+\rho_o^{-1}(w_{,1}-a_{<1>}))\right\}_{,1}+$$
$$\left\{\frac{2\varepsilon G}{\sin\vartheta}(\sin\vartheta\,\varphi_{<2>}+\rho_o^{-1}(w_{,2}-\sin\vartheta\,a_{<2>}))\right\}_{,2}+$$
$$-\ \frac{2\varepsilon}{\rho_o}\frac{E_p}{\Delta}\,\{(1+\nu_p)(\sin\vartheta(a_{<1>,1}+w)+\sin\vartheta\,w+a_{<2>,2}+\cos\vartheta\,a_{<1>})+$$
$$+\ 2(1+\nu_p\nu_{np})\rho_o\sin\vartheta\,\gamma\}+\rho_o\sin\vartheta\ q_o^{ni}{}_{<3>}=2\varepsilon\rho_o\delta_o\sin\vartheta\left\{\left(1+\frac{\varepsilon^2}{3\rho_o^2}\right)\ddot{w}+\frac{2\varepsilon^2}{3\rho_o}\ddot{\gamma}\right\},\tag{4.28}$$

$$
\begin{aligned}
&\{\frac{2\varepsilon^3}{3\rho_o}\frac{E_p}{\Delta}\sin\vartheta[(1-\nu_{pn}\nu_{np})(\varphi_{<1>,1}+\gamma)+\frac{\nu_p+\nu_{pn}\nu_{np}}{\sin\vartheta}(\varphi_{<2>,2}+\cos\vartheta\,\varphi_{<1>}+\\
&+\sin\vartheta\,\gamma)+(1+\nu_p)\nu_{np}\gamma]\}_{,1}+\{\frac{\varepsilon^3 E_p}{3\rho_o\sin\vartheta(1+\nu_p)}(\varphi_{<1>,2}-\cos\vartheta\,\varphi_{<2>}+\\
&+\sin\vartheta\,\varphi_{<2>,1})\}_{,2}-\frac{2\varepsilon^3\cos\vartheta}{3\rho_o}\frac{E_p}{\Delta}\{(\nu_p+\nu_{pn}\nu_{np})(\varphi_{<1>,1}+\gamma)+\\
&+\frac{1-\nu_{pn}\nu_{np}}{\sin\vartheta}(\varphi_{<2>,2}+\cos\vartheta\,\varphi_{<1>}+\sin\vartheta\,\gamma)+(1+\nu_p)\nu_{np}\,\gamma\}+\\
&-2\varepsilon\rho_o\sin\vartheta\,G(\varphi_{<1>}+\rho_o^{-1}(w_{,1}-a_{<1>}))+\rho_o\sin\vartheta\;r_o^{ni}{}_{<1>}=\\
&=2\varepsilon^3\delta_o\sin\vartheta\left\{\frac{2}{3}\ddot{a}_{<1>}+\rho_o\left(\frac{1}{3}+\frac{\varepsilon^2}{5\rho_o^2}\right)\ddot{\varphi}_{<1>}\right\},
\end{aligned}
\tag{4.29}
$$

$$
\begin{aligned}
&\left\{\frac{\varepsilon^3 E_p}{3\rho_o(1+\nu_p)}(\varphi_{<1>,2}-\cos\vartheta\,\varphi_{<2>}+\sin\vartheta\,\varphi_{<2>,1})\right\}_{,1}+\\
&\{\frac{2\varepsilon^3}{3\rho_o}\frac{E_p}{\Delta}[(\nu_p+\nu_{pn}\nu_{np})(\varphi_{<1>,1}+\gamma)+\frac{1-\nu_{pn}\nu_{np}}{\sin\vartheta}(\varphi_{<2>,2}+\cos\vartheta\,\varphi_{<1>}+\sin\vartheta\,\gamma)+\\
&+\;(1+\nu_p)\nu_{np}\,\gamma]\}_{,2}+\frac{\varepsilon^3 E_p\cot\vartheta}{3\rho_o(1+\nu_p)}(\varphi_{<1>,2}-\cos\vartheta\,\varphi_{<2>}+\sin\vartheta\,\varphi_{<2>,1})+\\
&-2\varepsilon\rho_o G(\sin\vartheta\,\varphi_{<2>}+\rho_o^{-1}(w_{,2}-\sin\vartheta\,a_{<2>}))+\rho_o\sin\vartheta\;r_o^{ni}{}_{<2>}=\\
&=2\varepsilon^3\delta_o\sin\vartheta\left\{\frac{2}{3}\ddot{a}_{<2>}+\rho_o\left(\frac{1}{3}+\frac{\varepsilon^2}{5\rho_o^2}\right)\ddot{\varphi}_{<2>}\right\},
\end{aligned}
\tag{4.30}
$$

$$
\begin{aligned}
&\left(\frac{2\varepsilon^3 G\sin\vartheta}{3\rho_o}\gamma_{,1}\right)_{,1}+\left(\frac{2\varepsilon^3 G}{3\rho_o\sin\vartheta}\gamma_{,2}\right)_{,2}-\frac{2\varepsilon^3\sin\vartheta}{3\rho_o}\frac{E_p}{\Delta}\{(1+\nu_p)(\varphi_{<1>,1}+\gamma)+\\
&+\frac{1+\nu_p}{\sin\vartheta}(\varphi_{<2>,2}+\cos\vartheta\,\varphi_{<1>}+\sin\vartheta\,\gamma)+2(1+\nu_p)\nu_{np}\,\gamma\}\\
&-2\varepsilon\frac{E_n}{\Delta}\{(1+\nu_p)\nu_{pn}[(a_{<1>,1}+w+\frac{\varepsilon^2}{3\rho_o}(\varphi_{<1>,1}+\gamma))\sin\vartheta+\\
&+a_{<2>,2}+\cos\vartheta\,a_{<1>}+\sin\vartheta\,w+\frac{\varepsilon^2}{3\rho_o}(\varphi_{<2>,2}+\cos\vartheta\,\varphi_{<1>}+\\
&+\sin\vartheta\,\gamma)]+(1-\nu_p^2)\left(1+\frac{\varepsilon^2}{3\rho_o^2}\right)\rho_o\sin\vartheta\,\gamma\}+\rho_o\sin\vartheta\;r_o^{ni}{}_{<3>}=\\
&=2\varepsilon^3\delta_o\sin\vartheta\left\{\frac{2}{3}\ddot{w}+\rho_o\left(\frac{1}{3}+\frac{\varepsilon^2}{5\rho_o^2}\right)\ddot{\gamma}\right\}.
\end{aligned}
\tag{4.31}
$$

This system of equations is to be equipped with a set of initial conditions for the unknown fields and for their time rates.

# Part II

# Analysis of Natural Vibrations

# Chapter 5

# Evolution Equations

In this chapter, we write down the evolution equations necessary to perform analysis of vibrational modes of a spherical shell, like the STMV capsid. To this aim, no external loads have to be taken into account, except the inertial distance force $\boldsymbol{d}_o^{in}$; therefore, the only distance actions per unit area involved are $\boldsymbol{q}_o = \boldsymbol{q}_o^{in}$ and $\boldsymbol{r}_o = \boldsymbol{r}_o^{in}$. Furthermore, as is the case in the majority of the literature about spherical capsids, we will restrict our attention to the subcase of homogeneous and isotropic response, as well as uniform thickness. Thus, equations (4.26) to (4.31) have to be specialized by neglecting the terms $q_o^{ni}{}_{<i>}$ and $r_o^{ni}{}_{<i>}$ $(i = 1, 2, 3)$ and assuming the elastic moduli to be independent of $x$, with $E_p = E_n = E$, $\nu_p = \nu_{pn} = \nu_{np} = \nu$, $E = 2G(1+\nu)$. Provided the above hypotheses, the general equations of Section 4.4 become:

$$
\begin{aligned}
&\frac{2E}{\rho_o(1+\nu)(1-2\nu)}\left[(1-\nu)(a_{<1>,1}+w)\sin\vartheta+\nu(\sin\vartheta\, w+a_{<2>,2}+\cos\vartheta\, a_{<1>})+\right.\\
&\left.\nu\rho_o\sin\vartheta\,\gamma\right]_{,1}+\frac{E}{\rho_o\sin\vartheta(1+\nu)}(a_{<1>,2}-\cos\vartheta\, a_{<2>}+\sin\vartheta\, a_{<2>,1})_{,2}+\\
&-\frac{2\cot\vartheta}{\rho_o}\frac{E}{(1+\nu)(1-2\nu)}\left[\nu\sin\vartheta(a_{<1>,1}+w)+(1-\nu)(\sin\vartheta\, w+a_{<2>,2}+\right.\\
&\left.\cos\vartheta\, a_{<1>})+\nu\rho_o\sin\vartheta\,\gamma\right]+2G\sin\vartheta(\varphi_{<1>}+\rho_o^{-1}(w_{,1}-a_{<1>}))=\\
&=2\rho_o\delta_o\sin\vartheta\,\left[\left(1+\frac{\varepsilon^2}{3\rho_o^2}\right)\ddot{a}_{<1>}+\frac{2\varepsilon^2}{3\rho_o}\ddot{\varphi}_{<1>}\right],
\end{aligned}
\tag{5.1}
$$

$$\frac{E}{\rho_o(1+\nu)}(a_{<1>,2}-\cos\vartheta\, a_{<2>}+\sin\vartheta\, a_{<2>,1}\,)_{,1}+$$
$$\frac{2E}{\rho_o\sin\vartheta(1+\nu)(1-2\nu)}[\nu\sin\vartheta(a_{<1>,1}+w)+(1-\nu)(\sin\vartheta\, w+a_{<2>,2}+\cos\vartheta\, a_{<1>})+$$
$$+\nu\rho_o\sin\vartheta\,\gamma]_{,2}+\frac{E\cot\vartheta}{\rho_o(1+\nu)}(a_{<1>,2}-\cos\vartheta\, a_{<2>}+\sin\vartheta\, a_{<2>,1}\,)+$$
$$+2G(\sin\vartheta\,\varphi_{<2>}+\rho_o^{-1}(w_{,2}-\sin\vartheta\, a_{<2>}))=2\rho_o\delta_o\sin\vartheta\left[\left(1+\frac{\varepsilon^2}{3\rho_o^2}\right)\ddot{a}_{<2>}+\frac{2\varepsilon^2}{3\rho_o}\ddot{\varphi}_{<2>}\right], \tag{5.2}$$

$$G\left[\sin\vartheta(\varphi_{<1>}+\rho_o^{-1}(w_{,1}-a_{<1>}))\right]_{,1}+\frac{G}{\sin\vartheta}\left[\sin\vartheta\,\varphi_{<2>}+\rho_o^{-1}(w_{,2}-\sin\vartheta\, a_{<2>})\right]_{,2}+$$
$$-\frac{E}{\rho_o(1+\nu)^2(1-2\nu)}\left[(1+\nu)(\sin\vartheta(a_{<1>,1}+w)+\sin\vartheta\, w+a_{<2>,2}+\cos\vartheta\, a_{<1>})+\right.$$
$$\left.2(1+\nu^2)\rho_o\sin\vartheta\,\gamma\right]=\rho_o\delta_o\sin\vartheta\left[\left(1+\frac{\varepsilon^2}{3\rho_o^2}\right)\ddot{w}+\frac{2\varepsilon^2}{3\rho_o}\ddot{\gamma}\right], \tag{5.3}$$

$$\frac{2\varepsilon^2E\sin\vartheta}{3\rho_o(1+\nu)(1-2\nu)}\left[(1-\nu)(\varphi_{<1>,1}+\gamma)+\frac{\nu}{\sin\vartheta}(\varphi_{<2>,2}+\cos\vartheta\,\varphi_{<1>}+\sin\vartheta\,\gamma)+\nu\gamma\right]_{,1}+$$
$$\frac{\varepsilon^2E}{3\rho_o\sin\vartheta(1+\nu)}(\varphi_{<1>,2}-\cos\vartheta\,\varphi_{<2>}+\sin\vartheta\,\varphi_{<2>,1}\,)_{,2}+$$
$$-\frac{2\varepsilon^2E\cos\vartheta}{3\rho_o(1+\nu)(1-2\nu)}\left[\nu(\varphi_{<1>,1}+\gamma)+\frac{1-\nu}{\sin\vartheta}(\varphi_{<2>,2}+\cos\vartheta\,\varphi_{<1>}+\sin\vartheta\,\gamma)+\nu\gamma\right]+$$
$$-2\rho_oG\sin\vartheta(\varphi_{<1>}+\rho_o^{-1}(w_{,1}-a_{<1>}))=2\varepsilon^2\delta_o\sin\vartheta\left[\frac{2}{3}\ddot{a}_{<1>}+\rho_o\left(\frac{1}{3}+\frac{\varepsilon^2}{5\rho_o^2}\right)\ddot{\varphi}_{<1>}\right], \tag{5.4}$$

$$\frac{\varepsilon^2E}{3\rho_o(1+\nu)}(\varphi_{<1>,2}-\cos\vartheta\,\varphi_{<2>}+\sin\vartheta\,\varphi_{<2>,1}\,)_{,1}+$$
$$+\frac{2\varepsilon^2E}{3\rho_o(1+\nu)(1-2\nu)}\left[\nu(\varphi_{<1>,1}+\gamma)+\frac{1-\nu}{\sin\vartheta}(\varphi_{<2>,2}+\cos\vartheta\,\varphi_{<1>}+\sin\vartheta\,\gamma)+\nu\gamma\right]_{,2}+$$
$$\frac{\varepsilon^2E\cot\vartheta}{3\rho_o(1+\nu)}(\varphi_{<1>,2}-\cos\vartheta\,\varphi_{<2>}+\sin\vartheta\,\varphi_{<2>,1}\,)+$$
$$-2G(\rho_o\sin\vartheta\,\varphi_{<2>}+w_{,2}-\sin\vartheta\, a_{<2>})=2\varepsilon^2\delta_o\sin\vartheta\left[\frac{2}{3}\ddot{a}_{<2>}+\rho_o\left(\frac{1}{3}+\frac{\varepsilon^2}{5\rho_o^2}\right)\ddot{\varphi}_{<2>}\right], \tag{5.5}$$

$$\frac{\varepsilon^2 G}{3\rho_o}(\sin\vartheta\,\gamma_{,1}\,)_{,1}+\frac{\varepsilon^3 G}{3\rho_o\sin\vartheta}\gamma_{,22}-\frac{\varepsilon^2 E\sin\vartheta}{3\rho_o(1+\nu)(1-2\nu)}[\varphi_{<1>}+\gamma+\frac{1}{\sin\vartheta}(\varphi_{<2>,2}+$$
$$\cos\vartheta\,\varphi_{<1>}+\sin\vartheta\,\gamma)+2\nu\gamma]-\frac{E}{(1+\nu)(1-2\nu)}\{\nu[(a_{<1>,1}+w+\frac{\varepsilon^2}{3\rho_o}(\varphi_{<1>,1}+\gamma))\sin\vartheta+$$
$$+a_{<2>,2}+\cos\vartheta\,a_{<1>}+\sin\vartheta\,w+\frac{\varepsilon^2}{3\rho_o}(\varphi_{<2>,2}+\cos\vartheta\,\varphi_{<1>}+\sin\vartheta\,\gamma)]+$$
$$(1-\nu)\left(1+\frac{\varepsilon^2}{3\rho_o^2}\right)\rho_o\sin\vartheta\,\gamma\}=\varepsilon^2\delta_o\sin\vartheta\left[\frac{2}{3}\ddot{w}+\rho_o\left(\frac{1}{3}+\frac{\varepsilon^2}{5\rho_o^2}\right)\ddot{\gamma}\right]. \tag{5.6}$$

## 5.1 Analytical Solutions

In this section, we examine some special cases in which it is possible to write down closed-form solutions of equations (5.1) to (5.6) that represent vibrational modes of a spherical shell. We restrict our attention to *axisymmetric vibrations*, so that all derivatives of the scalar kinematical parameters with respect to $\psi$ vanish; we also denote differentiation with respect to $\vartheta$ (the only spatial variable involved) by a prime. We can represent the general axisymmetric displacement field in terms of the elements of the physical basis as follows:

$$\begin{aligned}\boldsymbol{u}_a(\vartheta,\psi,\zeta,t)=&(a_{<1>}(\vartheta,t)+\zeta\varphi_{<1>}(\vartheta,t))\,\boldsymbol{e}_{<1>}(\vartheta,\psi)+\\&+(a_{<2>}(\vartheta,t)+\zeta\varphi_{<2>}(\vartheta,t))\,\boldsymbol{e}_{<2>}(\psi)+(w(\vartheta,t)+\zeta\gamma(\vartheta,t))\,\boldsymbol{n}(\vartheta,\psi).\end{aligned} \tag{5.7}$$

### 5.1.1 Radial Vibrations without Thickness Changes

The scalar parameter which describes radial displacements is $w$. Since we only have this unknown (all other parameter fields in (5.7) being taken identically null), all variations of the kinematical parameters appearing in the weak formulation (4.7) vanish, except $\delta w$. Therefore, the equation that governs the evolution of $w$ is (5.3), which takes the following form:

$$G(w''+\cot\vartheta\;w')-\frac{2E}{(1+\nu)(1-2\nu)}w=\rho_o^2\delta_o\left(1+\frac{\varepsilon^2}{3\rho_o^2}\right)\ddot{w}. \tag{5.8}$$

It is immediate to check that, if $w$ is independent of $\vartheta$, then (5.8) reads

$$\ddot{w} + \omega_0^2 w = 0, \quad \text{with} \quad \omega_0^2 = \frac{2E}{\rho_o^2 \delta_o \left(1 + \frac{\varepsilon^2}{3\rho_o^2}\right)(1+\nu)(1-2\nu)};$$

this special case corresponds to uniform radial vibrations (shrinking or swelling of the shell). More generally, if we look for solutions of the form

$$w(\vartheta, t) = \widehat{w}(\vartheta) \cos \omega t, \tag{5.9}$$

we see that the same vibrational frequency $\omega_0$ is associated with radial displacements whose spatial dependence is such that the first addend on the left-hand side of (5.8) vanishes, i.e.,

$$\widehat{w}'' + \cot \vartheta \ \widehat{w}' = 0.$$

The general solution of this equation can be readily found by separation of variables, and turns out to be

$$\widehat{w}(\vartheta) = c_1 \log \left( \tan \frac{\vartheta}{2} \right) + c_2, \tag{5.10}$$

with $c_1$ and $c_2$ two integration constants. This solution diverges as $\vartheta \to 0^+$ and $\vartheta \to \pi^-$, and is null at $\vartheta = \frac{\pi}{2}$.

Another solution of (5.8), obtained by using factorization (5.9), is given by

$$\widehat{w}(\vartheta) = a \cos \vartheta, \quad a = \text{a constant}. \tag{5.11}$$

In this case, the vibrational frequency turns out to be

$$\omega_1^2 = \frac{2G(3-2\nu)}{\rho_o^2 \delta_o \left(1 + \frac{\varepsilon^2}{3\rho_o^2}\right)(1-2\nu)} = \frac{E(3-2\nu)}{\rho_o^2 \delta_o \left(1 + \frac{\varepsilon^2}{3\rho_o^2}\right)(1+\nu)(1-2\nu)}.$$

Since $-1 < \nu < \frac{1}{2}$, it results that $\omega_1^2 > \omega_0^2$. For any fixed time $t$, the radial

displacement is maximum in magnitude at the two poles ($\vartheta = 0$ and $\vartheta = \pi$) and null at $\vartheta = \frac{\pi}{2}$ (Fig. 5.1).

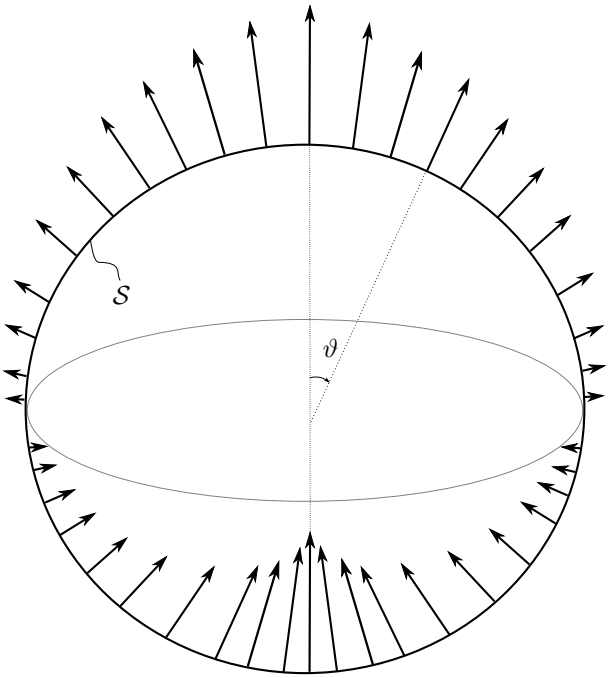


Figure 5.1: Radial displacements given by (5.11), with $a > 0$.

### 5.1.2 Uniform Radial Vibrations with Thickness Changes

In this case, we have two unknown fields: $w$ and $\gamma$. Applying the same argument as in the previous case, we have to consider equations (5.3) and (5.6). As we are interested in uniform radial and thickness vibrations, we look for solutions of the form

$$w = \widehat{w}\cos(\omega t), \quad \gamma = \widehat{\gamma}\cos(\omega t),$$

with $\widehat{w}$ and $\widehat{\gamma}$ constants. With these hypotheses, equation (5.3) reads

$$-\omega^2\rho_o^2\delta_o\left(\left(1+\frac{\varepsilon^2}{3\rho_o^2}\right)\widehat{w}+\frac{2\varepsilon^2}{3\rho_o}\widehat{\gamma}\right)+\frac{2E}{(1+\nu)^2(1-2\nu)}\left((1+\nu)\widehat{w}+(1+\nu^2)\rho_o\widehat{\gamma}\right)=0, \tag{5.12}$$

whereas (5.6) takes the form

$$\begin{aligned}&-\omega^2\varepsilon^2\delta_o\left(\frac{2}{3}\widehat{w}+\rho_o\left(\frac{1}{3}+\frac{\varepsilon^2}{5\rho_o^2}\right)\widehat{\gamma}\right)+\\&+\frac{E}{1-2\nu}\left\{\frac{2\varepsilon^2}{3\rho_o}\widehat{\gamma}+\frac{1}{1+\nu}\left[2\nu\widehat{w}+\left((1-\nu)\rho_o+(1+\nu)\frac{\varepsilon^2}{3\rho_o}\right)\widehat{\gamma}\right]\right\}=0.\end{aligned}\tag{5.13}$$

Thus, we find two expressions of $\omega^2$ in terms of $\widehat{w}$ and $\widehat{\gamma}$; we then need to solve the following algebraic equation:

$$\begin{aligned}&\frac{2E\left((1+\nu)\widehat{w}+(1+\nu^2)\rho_o\widehat{\gamma}\right)}{\rho_o^2\delta_o(1+\nu)^2(1-2\nu)\left(\left(1+\frac{\varepsilon^2}{3\rho_o^2}\right)\widehat{w}+\frac{2\varepsilon^2}{3\rho_o}\widehat{\gamma}\right)}\\&\qquad=\frac{\frac{E}{1-2\nu}\left\{\frac{2\varepsilon^2}{3\rho_o}\widehat{\gamma}+\frac{1}{1+\nu}\left[2\nu\widehat{w}+\left((1-\nu)\rho_o+(1+\nu)\frac{\varepsilon^2}{3\rho_o}\right)\widehat{\gamma}\right]\right\}}{\varepsilon^2\delta_o\left(\frac{2}{3}\widehat{w}+\rho_o\left(\frac{1}{3}+\frac{\varepsilon^2}{5\rho_o^2}\right)\widehat{\gamma}\right)}.\end{aligned}$$

This equation has the form

$$\frac{a\widehat{w}+b\widehat{\gamma}}{c\widehat{w}+d\widehat{\gamma}}=\frac{e\widehat{w}+g\widehat{\gamma}}{h\widehat{w}+k\widehat{\gamma}}\iff(dg-bk)\widehat{\gamma}^2+(cg+de-ak-bh)\widehat{w}\widehat{\gamma}+(ce-ah)\widehat{w}^2=0,\tag{5.14}$$

with

$$\begin{aligned}&a:=2E(1+\nu),\quad b:=2E(1+\nu^2)\rho_o,\\&c:=\rho_o^2\delta_o\left(1+\frac{\varepsilon^2}{3\rho_o^2}\right)(1+\nu)^2(1-2\nu),\quad d:=\frac{2}{3}\varepsilon^2\rho_o\delta_o(1+\nu)^2(1-2\nu),\\&e:=\frac{2E\nu}{(1+\nu)(1-2\nu)},\\&g:=\frac{E}{1-2\nu}\left(\frac{\varepsilon^2}{\rho_o}+\frac{1-\nu}{1+\nu}\rho_o\right),\\&h:=\frac{2}{3}\varepsilon^2\delta_o,\quad k:=\varepsilon^2\rho_o\delta_o\left(\frac{1}{3}+\frac{\varepsilon^2}{5\rho_o^2}\right).\end{aligned}$$

The solutions of (5.14) are

$$\begin{aligned}&\widehat{\gamma}_\pm=K_\pm\widehat{w},\quad\text{with}\\&K_\pm:=\frac{ak+bh-de-cg\pm\sqrt{(ak+bh-de-cg)^2-4(dg-bk)(ce-ah)}}{2(dg-bk)};\end{aligned}$$

hence, in this case, the shell has two vibrational frequencies:

$$\omega_{\pm}^2 := \frac{2E\left((1+\nu)+(1+\nu^2)\rho_o K_{\pm}\right)}{\rho_o^2\delta_o(1+\nu)^2(1-2\nu)\left(\left(1+\frac{\varepsilon^2}{3\rho_o^2}\right)+\frac{2\varepsilon^2}{3\rho_o}K_{\pm}\right)}.$$

### 5.1.3 Parallel-Wise Twist Vibrations

By parallel-wise displacements we mean displacements along the directions tangent to the parallel curves $\vartheta = \text{const}$ on the middle surface, i.e., along the direction of the vector field $\boldsymbol{e}_{<2>}$. Thus, the only scalar parameter to be taken into account in this case is $a_{<2>}$, and the governing equation is (5.2), which reads:

$$a_{<2>}'' + \cot\vartheta\ a_{<2>}' - \cot^2\vartheta\ a_{<2>} = \frac{\rho_o^2\delta_o}{G}\left(1+\frac{\varepsilon^2}{3\rho_o^2}\right)\ddot{a}_{<2>}. \tag{5.15}$$

Again, with a view toward solving this PDE, we tentatively write:

$$a_{<2>}(\vartheta,t) = \widehat{a}_{<2>}(\vartheta)\cos\omega t,$$

and quickly find that, on choosing a twisting displacement of the form:

$$\widehat{a}_{<2>}(\vartheta) = a\sin\vartheta\cos\vartheta, \quad a = \text{a constant}, \tag{5.16}$$

$a_{<2>}$ solves (5.15) with

$$\omega^2 = \frac{5G}{\rho_o^2\delta_o\left(1+\frac{\varepsilon^2}{3\rho_o^2}\right)} = \frac{5E}{2\rho_o^2\delta_o\left(1+\frac{\varepsilon^2}{3\rho_o^2}\right)(1+\nu)}.$$

For any fixed time $t$, the displacement is maximum in magnitude at $\vartheta = \frac{\pi}{4}$ and $\vartheta = \frac{3}{4}\pi$, and null for $\vartheta = \frac{\pi}{2}$ (Fig. 5.2); note also that, although $\boldsymbol{e}_{<2>}$ is not defined for $\vartheta = 0$ and $\vartheta = \pi$, we have

$$\lim_{\vartheta\to 0^+} a_{<2>}(\vartheta,t) = \lim_{\vartheta\to\pi^-} a_{<2>}(\vartheta,t) = 0.$$

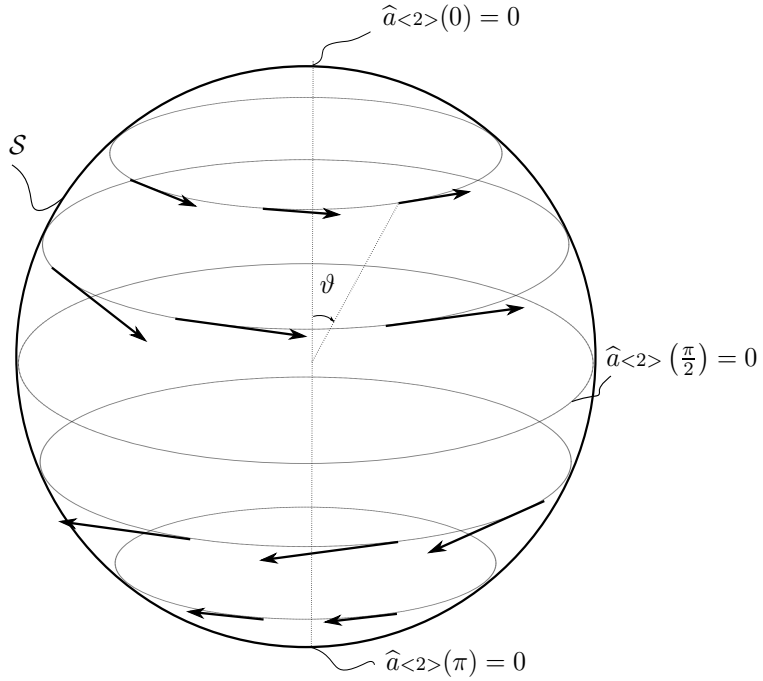


Figure 5.2: Parallel-wise twist displacements given by (5.16), with $a > 0$.

### 5.1.4 Parallel-Wise Shear Vibrations

The last type of vibrational mode we examine is a shear vibration along the direction $\boldsymbol{e}_{<2>}$, in which transversal fibers rotate about their mid point on the middle surface, which does not move (Fig. 5.3). In these circumstances, the only nonzero scalar parameter field is $\varphi_{<2>}$, whose evolution is ruled by equation (5.5), which becomes:

$$\frac{\varepsilon^2}{\rho_o^2}\left(\varphi_{<2>}{}'' + \cot\vartheta\ \varphi_{<2>}{}' + (1-\cot^2\vartheta)\,\varphi_{<2>}\right) - 3\,\varphi_{<2>} = \frac{\varepsilon^2\delta_o}{G}\left(1+\frac{3}{5}\,\frac{\varepsilon^2}{\rho_o^2}\right)\ddot{\varphi}_{<2>}. \tag{5.17}$$

Note that, if $\varepsilon$ and $\rho_o$ are given the values measured by Yang et al. [28], i.e., $\varepsilon = 15.3\,\text{Å}$ and $\rho_o = 70.7\,\text{Å}$, then $\frac{3\varepsilon^2}{5\rho_o^2} \approx 0.024$; hence, if this term is neglected with respect to 1, we get an approximated expression of the shear vibrational frequency, that does not depend on the radius of the middle surface:

$$\widetilde{\omega}^2 = \frac{3G}{\varepsilon^2\delta_o} = \frac{3E}{2\varepsilon^2\delta_o(1+\nu)}.$$

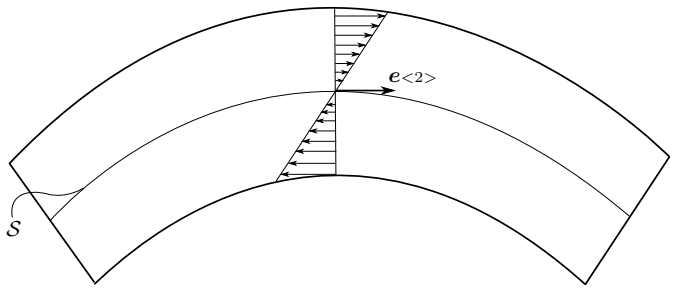


Figure 5.3: Parallel-wise shear displacements.

On the other hand, if we consider the exact equation, we find that

$$\varphi_{<2>}(\vartheta, t) = \widehat{\varphi}_{<2>}(\vartheta)\cos\omega t, \quad \text{with} \quad \widehat{\varphi}_{<2>}(\vartheta) = a\,\sin\vartheta,$$

solves (5.17) with

$$\omega^2 = \frac{G}{3\delta_o\,\varepsilon^2\left(1+\frac{3}{5}\,\frac{\varepsilon^2}{\rho_o^2}\right)} = \frac{E}{6\delta_o\varepsilon^2\left(1+\frac{3}{5}\,\frac{\varepsilon^2}{\rho_o^2}\right)(1+\nu)}.$$

Analogously to the previous case, the shear tends to vanish at $\vartheta = 0$ and $\vartheta = \pi$ and attains its maximum at $\vartheta = \frac{\pi}{2}$.

In both the approximated and exact cases, we see that the vibrational frequency diverges as $\varepsilon \to 0$: inducing a parallel-wise shear vibrational mode, and measuring the corresponding frequency, would be very difficult and perhaps also scarcely conclusive.

# Chapter 6

# Directions for Future Research

## 6.1 Multiscale Modeling of Spherical Capsids

A relevant open problem is the construction of a suitable multiscale mechanical model for *spherical capsids*. By multiscale model we mean a bottom-up sequence of modeling steps, from Molecular Dynamics to Continuum Mechanics, via an intermediate *coarse-grained* model. Such a sequence aims to correlate the interactions of capsid particles at the nanoscopic scale with the elastic moduli characterizing a capsid at the macroscopic scale (the Young's modulus and the Poisson's ratio, or the six technical moduli defined in Section 4.3, according to whether the capsid is thought of as isotropic or transversely isotropic, respectively). The scale described by the coarse-grained model can be termed *meta-nanoscopic*. For example, as it has been done for carbon nanotubes [4], a bridge between the continuum and atomistic scales could be built up by assuming energy conservation between scales: equating the continuum stored elastic energy to the coarse-grained stored elastic energy provides relationships between the elastic moduli and the parameters of the coarse-grained model; furthermore, values of these parameters should be inferred from Molecular Dynamics simulations or experimental procedures, thus completing the scale bridging.

As to *protein assemblies*, Freddolino et al. [8] performed Molecular Dynamics

simulations of a whole STMV (RNA plus capsid assembly) and of its capsid alone. As to coarse-grained models that can be applied to the study of such structures, two examples (both belonging to the category of the Elastic Network Models) are the Anisotropic Network Model and the Gaussian Network Model [1, 6].

## 6.2 Full Capsids in a Hydrostatic Environment

Another open problem consists in studying the vibrations of a full spherical capsid placed in a hydrostatic environment. In this case, beside the inertial distance force, the load system acting on the capsid consists also of

(*i*) an internal pressure, exerted by the genome packed inside the shell;

(*ii*) an external pressure exerted by the solvent in which the capsid floats.

Both these pressure fields are uniform in magnitude and both are 'live' loads, in the sense that their direction depends on the motion and that, moreover, the magnitude of the internal pressure depends on the current volume of the cavity filled by the genome. The referential counterparts of the internal and the external pressures are represented, respectively, by the surface contact loads $\boldsymbol{c}_o^-(x,t)$ and $\boldsymbol{c}_o^+(x,t)$ (cf. subsection 4.1.2; here, we add time dependence to stress the fact that these loads depend on the motion of the body). In the following two subsections, we specify how these loads are related to the motion of the shell. To this aim, we resort to the procedure set forth in [20].

Consider the *motion* of the shell-like region $\mathcal{G}$, given by the mapping

$$\mathcal{G} \ni p \mapsto y(p,t) = p + \boldsymbol{u}(p,t) \in \mathcal{E},$$

with $\boldsymbol{u}$ as in (3.1). We call $\boldsymbol{Y}(p,t) := \nabla y(p,t)$ the *motion gradient*. We have that

$$\boldsymbol{Y}(p,t) = \boldsymbol{I} + \boldsymbol{H}(p,t),$$

where $\boldsymbol{H} := \nabla \boldsymbol{u}$ is the displacement gradient and $\boldsymbol{I}$ is the identity tensor on $\mathcal{V}$. We presume, as usual, $\det \boldsymbol{Y} > 0$ in $\mathcal{G}$.

### 6.2.1 Genome Pressure

We may consider the genome behaving as a *compressible non-viscous fluid*; hence, it exerts on the current inner surface $y(\mathcal{S}^-, t)$ a pressure $\pi_i$ of magnitude inversely proportional to the volume of the three-dimensional region wrapped by $y(\mathcal{S}^-, t)$. Denoting this region by $\langle y(\mathcal{S}^-, t)\rangle$, we have

$$\pi_i = \chi \left(\operatorname{vol} \langle y(\mathcal{S}^-, t)\rangle\right)^{-1}, \tag{6.1}$$

where $\chi > 0$ is constant. Therefore, this pressure has a *non-local* character. If $\boldsymbol{m}$ and $\boldsymbol{n}$ are, respectively, the unit normal vector fields over $\mathcal{S}^-$ and $y(\mathcal{S}^-, t)$, it follows from the divergence theorem that

$$\operatorname{vol} \langle y(\mathcal{S}^-, t)\rangle = -\frac{1}{3}\int_{y(S^-,t)} \boldsymbol{y}\cdot\boldsymbol{m} = -\frac{1}{3}\int_{\mathcal{S}^-} (\boldsymbol{p}+\boldsymbol{u})\cdot \boldsymbol{Y}_*\boldsymbol{n}, \tag{6.2}$$

where we have set $\boldsymbol{y} := y - o$; $\boldsymbol{Y}_* := (\det \boldsymbol{Y})\boldsymbol{Y}^{-T}$ is the *cofactor*[1] of $\boldsymbol{Y}$, and $\boldsymbol{m} = |\boldsymbol{Y}_*\boldsymbol{n}|^{-1}\boldsymbol{Y}_*\boldsymbol{n}$. Thus, by the second equality of (6.2), we can rewrite (6.1) as

$$\pi_i = \kappa\left(\int_{\mathcal{S}^-} (\boldsymbol{p}+\boldsymbol{u})\cdot \boldsymbol{Y}_*\boldsymbol{n}\right)^{-1}, \quad \text{with} \quad \kappa := 3\chi.$$

The vector field representing this pressure in the referential configuration of the shell is given by

$$\boldsymbol{c}_o^-(x,t) = \pi_i\, \boldsymbol{Y}_*^-(x,t)\,\boldsymbol{n}(x) = \kappa\left(\int_{\mathcal{S}^-} (\boldsymbol{p}+\boldsymbol{u})\cdot \boldsymbol{Y}_*\boldsymbol{n}\right)^{-1} \boldsymbol{Y}_*^-(x,t)\,\boldsymbol{n}(x). \tag{6.3}$$

Now, as we assume small strains, linearization of $\boldsymbol{Y}_*$ in (6.3) with respect to the smallness parameter $e := |\boldsymbol{H}|$ is needed [19]. This linearization, after scaling

[1] Here, $\boldsymbol{Y}^{-T} := \left(\boldsymbol{Y}^T\right)^{-1}$.

back the resulting relation by letting $e = 1$, yields

$$\boldsymbol{Y}_* = \boldsymbol{I} + \tilde{\boldsymbol{H}}, \quad \text{with} \quad \tilde{\boldsymbol{H}} = (\operatorname{tr} \boldsymbol{H})\, \boldsymbol{I} - \boldsymbol{H}^T = (\operatorname{Div} \boldsymbol{u})\, \boldsymbol{I} - \nabla \boldsymbol{u}^T. \tag{6.4}$$

Thus, we finally obtain

$$\boldsymbol{c}_o^-(x,t) = \kappa \left\{ \int_{\mathcal{S}^-} (\boldsymbol{p} + \boldsymbol{u}) \cdot \Big( \boldsymbol{I} + \tilde{\boldsymbol{H}} \Big) \boldsymbol{n} \right\}^{-1} \Big( \boldsymbol{I} + \tilde{\boldsymbol{H}}^-(x,t) \Big)\, \boldsymbol{n}(x). \tag{6.5}$$

### 6.2.2 Solvent Pressure

The pressure exerted by the solvent on the current outer surface $y(\mathcal{S}^+, t)$ of the shell is uniform in magnitude, but its direction varies due to the variation of the normal direction with motion. Hence, this pressure has a *local* character. Again, this load is represented, in the referential configuration, by the vector

$$\boldsymbol{c}_o^+(x,t) = -\pi_o \boldsymbol{Y}_*^+(x,t) \boldsymbol{n}(x),$$

where $\pi_o > 0$ is constant. By linearization of $\boldsymbol{Y}_*^+$, we get

$$\boldsymbol{c}_o^+(x,t) = -\pi_o \Big( \boldsymbol{I} + \tilde{\boldsymbol{H}}^+(x,t) \Big)\, \boldsymbol{n}(x), \tag{6.6}$$

where $\tilde{\boldsymbol{H}}$ is defined as in (6.4).

Note that, because in this problem the loads $\boldsymbol{c}_o^+$ and $\boldsymbol{c}_o^-$ are nonzero, in addition to the inertial distance force $\boldsymbol{q}_o^{in}$ and couple $\boldsymbol{r}_o^{in}$, a non-inertial distance force $\boldsymbol{q}_o^{ni}$ and a non-inertial distance couple $\boldsymbol{r}_o^{ni}$ per unit area shall be present as well. In particular, equations (4.26) to (4.31) make up an *integro-differential* system, due to the fact that the pressure of the genome depends on the current volume of the cavity in which it is packed.

# Conclusions

We have addressed the problem of studying natural vibrations of spherical viral capsids (with particular reference to the STMV capsid) by employing a linear theory of elastic shells that accounts for thickness distension. Starting from the general assumption of transversely isotropic response with respect to the radial direction – an assumption that is thought to better reflect the rotational symmetries of the capsomers with respect to that direction – we have specialized the governing equations in the subcase of homogeneous and isotropic response, and we have found a few cases in which closed-form solutions can be arrived at. Such simple cases (among which, for example, radial and parallel-wise vibrations) might be considered as a reference to infer a correct evaluation of Young's modulus and Poisson's ratio for a spherical capsid, when thought of as an isotropic body, by carrying out experiments that induce the relative vibrational modes. We believe that this would be a major achievement, given that, in spite of the fact that capsids are rather thin, the available experiments are used in combination with formulae from three-dimensional linear elasticity that are only valid in bulk.

Finally, we have set forth two open problems: (*i*) to put together a multiscale mechanical model of spherical capsids, capable to bridge the atomistic and continuum scales, so as to yield a nanoscopically-informed continuum theory of such structures; (*ii*) to study the vibrations of full spherical capsids in a hydrostatic environment, thus by taking into account both the internal pressure, exerted by the genome that fills the shell cavity, and the external pressure,

exerted by the solvent on the outer surface of the capsid.

# Bibliography


[1] A. R. Atilgan, S. R. Durell, R. L. Jernigan, M. C. Demirel, O. Keskin, I. Bahar, Anisotropy of Fluctuation Dynamics of Proteins with an Elastic Network Model, Biophysical Journal, Volume 80, 505-515, 2001.

[2] C. Bajaj, Geometric Modeling and Quantitative Visualization of Virus Ultra-structure, Chap. 7 in *Modeling Biology: Structures, Behaviors, Evolution*, MIT Press 2006.

[3] C. Bajaj, B. Subramanian, W. Wang, Y. Li, Q. Zhang, Non-linear Continuum Elasticity Modeling of Viral Capsids, Forthcoming.

[4] C. Bajaj, A. Favata, P. Podio-Guidugli, On a Nanoscopically-Informed Shell Theory of Single-Wall Carbon Nanotubes, Preprint submitted to Journal of the Mechanics and Physics of Solids, 2011.

[5] D. L. D. Caspar, A. Klug, Physical Principles in the Construction of Regular Viruses, Cold Spring Harbor Symposia on Quantitative Biology, Volume XXVII, 1962.

[6] Q. Cui, I. Bahar, *Normal Mode Analysis: Theory And Applications to Biological and Chemical Systems*, CRC Press, 2006.

[7] A. Favata, P. Podio-Guidugli, A New CNT-Oriented Shell Theory, European Journal of Mechanics, Volume 35, 75-96, 2012.

[8] P. L. Freddolino, A. S. Arkhipov, S. B. Larson, A. McPherson, K. Schulten, Molecular Dynamics Simulations of the Complete Satellite Tobacco Mosaic Virus, Structure 14, 437-449, 2006.

[9] M. Gibbons, W. S. Klug, Nonlinear Finite Element Analysis of Nanoindentation of Viral Capsids, Phys. Rev. E. Stat. Nonlin. Soft Matter Phys, 2007.

[10] M. Gibbons, W. S. Klug, Mechanical modeling of viral capsids, J Mater Sci 42, 8995-9004, 2007.

[11] M. Gibbons, W. S. Klug, Influence of Nonuniform Geometry on Nanoindentation of Viral Capsids, Biophysical Journal, Volume 95, 3640-3649, 2008.

[12] T. Keef, A Symmetry Approach to Virus Structure and Assembly, PhD Thesis, University of York, Department of Mathematics, 2007.

[13] S. B. Larson, S. Koszelak, J. Day, A. Greenwood, J. A. Dodds, A. McPherson, Three-dimensional structure of satellite tobacco mosaic virus at 2.9 Å resolution. J. Mol. Biol. 231, 375391, 1993.

[14] S. B. Larson, J. Day, A. Greenwood, A. McPherson, Refined structure of satellite tobacco mosaic virus at 1.8 Å resolution, J. Mol. Biol. 277, 3759, 1998.

[15] A. Lwoff, T. F. Anderson, F. Jacob, Remarques sur les caractéristiques de la particule infectieuse, Ann. Inn. Pasteur, 1959.

[16] J. P. Michel, I. L. Ivanovska, M. M. Gibbons, W. S. Klug, C. M. Knobler, G. J. L. Wuite, C. F. Schmidt, Nanoindentation studies of full and empty viral capsids and the effects of capsid protein mutations on elasticity and strength, Proc. Nat. Acad. Sci., 103 (16), 6184-6189, 2006.

[17] P. Podio-Guidugli, P. Nardinocchi, *The Linear Theory of Elastic Shells*, Forthcoming.

[18] P. Podio-Guidugli, *Lezioni sulla teoria lineare dei gusci elastici sottili*, Masson, 1991.

[19] P. Podio-Guidugli, *A Primer in Elasticity*, Kluwer Academic Publishers, 2000.

[20] P. Podio-Guidugli, E. G. Virga, Sull'equilibrio di un involucro elastico pieno di gas, Atti Acc. Lincei Rend. fis. (8), 287-292, 1987.

[21] W. H. Roos, I. L. Ivanovska, A. Evilevitch, G. J. L. Wuite, Viral capsids: Mechanical characteristics, genome packaging and delivery mechanisms, Cell. Mol. Life Sci. 64, 1484-1497, 2007.

[22] C. Q. Ru, Buckling of empty spherical viruses under external pressure, Journal of Applied Physics 105, 2009.

[23] J. A. Speir, S. Munshi, G. Wang, T. S. Baker and J. E. Johnson, Structures of the native and swollen forms of cowpea chlorotic mottle virus determined by X-ray crystallography and cryo-electron microscopy, Structure 15, 63-78, 1995.

[24] B. Stephanidis, S. Adichtchev, P. Gouet, A. McPherson, A. Mermet, Elastic properties of viruses, Biophysical Journal, Volume 93, 1354-1359, 2007.

[25] F. Tama, C. L. Brooks, Diversity and Identity of Mechanical Properties of Icosahedral Viral Capsids Studied with Elastic Network Normal Mode Analysis, J. Mol. Biol. 345, 299-314, 2005.

[26] F. Tama, C. L. Brooks, The Mechanism and Pathway of pH Induced Swelling in Cowpea Chlorotic Mottle Virus, J. Mol. Biol. 318, 733-747, .2002.

[27] G. A. Vliegenthart, G. Gompper, Mechanical properties of icosahedral virus capsids, J. Computer-Aided Mater. Des. 14, 111-119, 2007.

[28] Z. Yang, I. Bahar, M. Widom, Vibrational Dynamics of Icosahedrally Symmetric Biomolecular Assemblies Compared with Predictions Based on Continuum Elasticity, Biophysical Journal, Volume 96, 4438-4448, 2009.

[29] R. Zandi, D. Reguera, R. F. Bruinsma, W. M. Gelbart, J. Rudnick, Origin of icosahedral symmetry in viruses, PNAS, vol. 101, 15556-15560, 2004.

[30] A. Zlotnick, Theoretical aspects of virus capsid assembly, J. Mol. Recognit. 18, 479-490, 2005.